J. Fluid Mech. (2007), *vol.* 572, *pp.* 189–217.
doi:10.1017/S0022112006003399 Printed in the United Kingdom

Interaction of a deep-water wave with a vertical cylinder: effect of self-excited vibrations on quantitative flow patterns

By M. OZGOREN† AND D. ROCKWELL

Department of Mechanical Engineering and Mechanics, 356 Packard Laboratory, 19 Memorial Drive West, Lehigh University, Bethlehem, PA 18015, USA
dor0@lehigh.edu

(Received 17 May 2005 and in revised form 14 July 2006)

Interaction of a deep-water wave with a cylinder gives rise to ordered patterns of the flow structure, which are quantitatively characterized using a technique of high-image-density particle image velocimetry. When the cylinder is stationary, the patterns of instantaneous flow structure take on increasingly complex forms for increasing Keulegan–Carpenter number KC. These patterns involve stacking of small-scale vorticity concentrations, as well as large-scale vortex shedding. The time-averaged consequence of these patterns involves, at sufficiently high KC, an array of vorticity concentrations about the cylinder.

When the lightly damped cylinder is allowed to undergo bidirectional oscillations, the trajectories can be classified according to ranges of KC. At low values of KC, the trajectory is elliptical, and further increases of KC allow, first of all, both elliptical and in-line trajectories as possibilities, followed by predominantly in-line and figure-of-eight oscillations at the largest value of KC.

Representations of the quantitative flow structure, in relation to the instantaneous cylinder position on its oscillation trajectory, show basic classes of patterns. When the trajectory is elliptical, layers of vorticity rotate about the cylinder surface, in accordance with rotation of the relative velocity vector of the wave motion with respect to the oscillating cylinder. Simultaneously, the patterns of streamline topology take the form of large-scale bubbles, which also rotate about the cylinder. When the cylinder trajectory is predominantly in-line with the wave motion, generic classes of vortex formation and shedding can be identified; they include sweeping of previously shed vorticity concentrations past the cylinder to the opposite side. Certain of these patterns are directly analogous to those from the stationary cylinder.

1. Introduction

The interaction of a free-surface wave with a vertical cylinder is representative of a variety of situations in the field of ocean engineering, whereby the cylinder takes the form of a riser in an offshore drilling platform, or a cable in an ocean monitoring system. Such interactions can give rise to substantial loading and, if the cylinder is elastic, or elastically mounted, complex forms of cylinder response can occur. Characterizations of both the loading and response are challenging, as the wave

† Permanent address: Department of Mechanical Engineering, Selcuk University, 42079, Konya, Turkey.

motion is oscillatory. That is, the wave velocity undergoes large excursions in both magnitude and direction, in contrast to the unidirectional flow of a steady current.

A wide variety of related investigations have provided considerable insight into wave–cylinder interaction. They extend from one-dimensional oscillations of a cylinder in quiescent fluid or, conversely, oscillations of fluid past a stationary cylinder, to the fully complex case of an actual wave past the cylinder. An overview of these classes of investigations is provided by Sumer & Fredsøe (1997).

Stationary cylinder in oscillatory flow. One-dimensional oscillatory flow past a stationary cylinder or, equivalently, one-dimensional oscillations of a cylinder in quiescent fluid, have yielded considerable insight. Sarpkaya & Isaacson (1981) provide an overview of early investigations, which extends over ranges of: Keulegan–Carpenter number $KC = U_m/f_w D$, in which U_m is the peak velocity amplitude of the flow past the cylinder, f_w is the wave frequency, and D is the diameter of the cylinder; and the Stokes number $f_w D^2/\nu$, in which ν is the kinematic viscosity. Representative investigations include those of Bearman *et al.* (1981), Honji (1981), Ikeda & Yamamoto (1981), Iwagaki, Asano & Nagai (1983), Williamson (1985*a*), Sarpkaya (1986), Obasaju, Bearman & Graham (1988) and Tatsuno & Bearman (1990). As a result of these investigations, the admissible vortex patterns that occur over a range of KC have been defined and, in selected studies, are related to the unsteady loading on the cylinder.

Stationary cylinder in wave. Yang & Rockwell (2002) considered interaction of an intermediate-depth wave with a vertical stationary cylinder, with emphasis on quantitative patterns of the spanwise flow structure, which exhibited various modes that could be related to the magnitude of the unsteady loading on the cylinder. In a subsequent study, which focused on the interaction of a deep-water wave with a cylinder, Yang & Rockwell (2004) and Ozgoren & Rockwell (2004) determined both the quasi-two-dimensional and three-dimensional patterns of the flow structure, in relation to the exponential decay of the wave amplitude with depth, and the magnitude of the unsteady loading on the cylinder. The basic features of qualitatively determined patterns of vortex formation, described in the investigations in the preceding section, are replicated well in the deep-water wave.

Transverse vibrations of cylinder. One-dimensional (non-orbital) oscillatory flow past an elastically supported cylinder, arranged such that only transverse vibrations could occur, has been addressed by Sarpkaya & Rajabi (1979), Bearman & Hall (1987), Sumer & Fredsøe (1988), and Kozakiewicz, Sumer & Fredsøe (1997). Most of these investigations emphasize the importance of the natural frequency f_n of the elastically mounted cylinder, the wave frequency f_w and the cylinder vibration frequency f_v.

Similar characterizations, but for the case of an elastically mounted cylinder in an actual free-surface wave, have been pursued by Angrilli & Cossalter (1982), Kaye & Maull (1993) and Hayashi & Chaplin (1998). All of these investigations found a resonant response at integer values of f_n/f_w, and, furthermore, Hayashi & Chaplin (1998) discovered that such a response can also occur at non-integer values, if the elastically mounted cylinder has sufficiently light damping.

In-line vibration of cylinder. Williamson (1985*b*) performed one-dimensional oscillatory experiments and predicted the resonant response of in-line vibrations. Li, Zhan & Lau (1997) considered both regular and random wave motion during an experimental and theoretical study for a horizontal elastically mounted cylinder. Anagnostopoulos, Iliadis & Ganoulis (1995) performed a numerical simulation of in-line oscillations in a one-dimensional wave and assessed the magnitude and phase of the in-line response.

Bidirectional vibrations. If simultaneous transverse and in-line vibrations are allowed to occur, bidirectional vibrations can arise, giving rise to complex forms of cylinder trajectories. A number of investigations have employed a rigid cylinder, which is attached to a bidirectional cantilevered joint, or an equivalently flexible joint. Investigations that employ this configuration include Sawaragi, Nakamura & Miki (1977), Isaacson & Maull (1981), Zedan *et al.* (1981), Borthwick & Herbert (1988), Kaye (1989) and Kaye & Maull (1993). Taken together, these investigations could demonstrate that a resonant response can occur at integer values of f_n/f_w, and, furthermore, a wide range of admissible trajectories can occur.

A somewhat different method of elastically mounting the cylinder, i.e. a spring system on either end, was employed in the investigation of Lipsett & Williamson (1991, 1994), who addressed the case of one-dimensional wave motion past the cylinder. They were able to classify the possible cylinder trajectories on maps of KC versus f_n/f_w, and showed that simple mathematical models allowed prediction of the limit cycle trajectories.

For those investigations described in the foregoing for which the mass-damping parameter $m^*\zeta$ is specified, values ranged from 0.044 to 0.44. Of all of the previous investigations of bidirectional oscillations, characterization of vortex patterns, in direct correspondence to the bidirectional trajectories of the cylinder, were pursued only by Sawaragi *et al.* (1977), Borthwick & Herbert (1988) and Kaye (1989), who qualitatively visualized the vortex pattern at the free surface. Downes & Rockwell (2003) employed a bidirectional apparatus, which maintained the cylinder vertical during its interaction with an incident wave. In this investigation, the mass-damping parameter was relatively small, with a value $m^*\zeta = 0.0062$. The wave was of the intermediate type, with very elongated particle trajectories, in contrast to the deep-water wave of interest herein. Moreover, only a single (butterfly) trajectory of the cylinder motion was considered; more basic orbital, in-line and figure-of-eight trajectories, were not addressed. Finally, the streamline topology and associated critical points were not examined.

Unresolved issues and objectives. Interaction of a deep-water wave with a cylinder can give rise to complex forms of vortex formation. Determination of quantitative patterns of the flow structure, over a range of Keulegan–Carpenter number KC, with direct comparison of cases of the stationary cylinder and a cylinder free to undergo bidirectional oscillations, has not been pursued. That is, depending upon the trajectory of the cylinder oscillation, substantial departures of the quantitative flow patterns from those associated with the stationary cylinder, may occur. Nevertheless, depending upon the instant at which the cylinder trajectory is considered, the intriguing possibility of correspondence of instantaneous flow patterns from the oscillating cylinder with those of the stationary cylinder may be attainable. Of course, the trajectory of the cylinder, say an elliptical versus in-line motion, is expected to dictate the degree to which layers or clusters of vorticity tend to remain attached to the periphery of the cylinder, as opposed to being shed from the cylinder surface. These, as well as the foregoing features, are intimately related to the phase relationship between the velocity U_c of the cylinder, the wave velocity U_w, and thereby the relative wave velocity U_R of the wave relative to the frame of the cylinder. The foregoing characteristics have not been investigated in a systematic fashion over a range of lower KC, with an emphasis on quantitative imaging of the flow structure. The objective of the present investigation is to address these aspects using a technique of quantitative imaging for the cases of both stationary and oscillating cylinders.

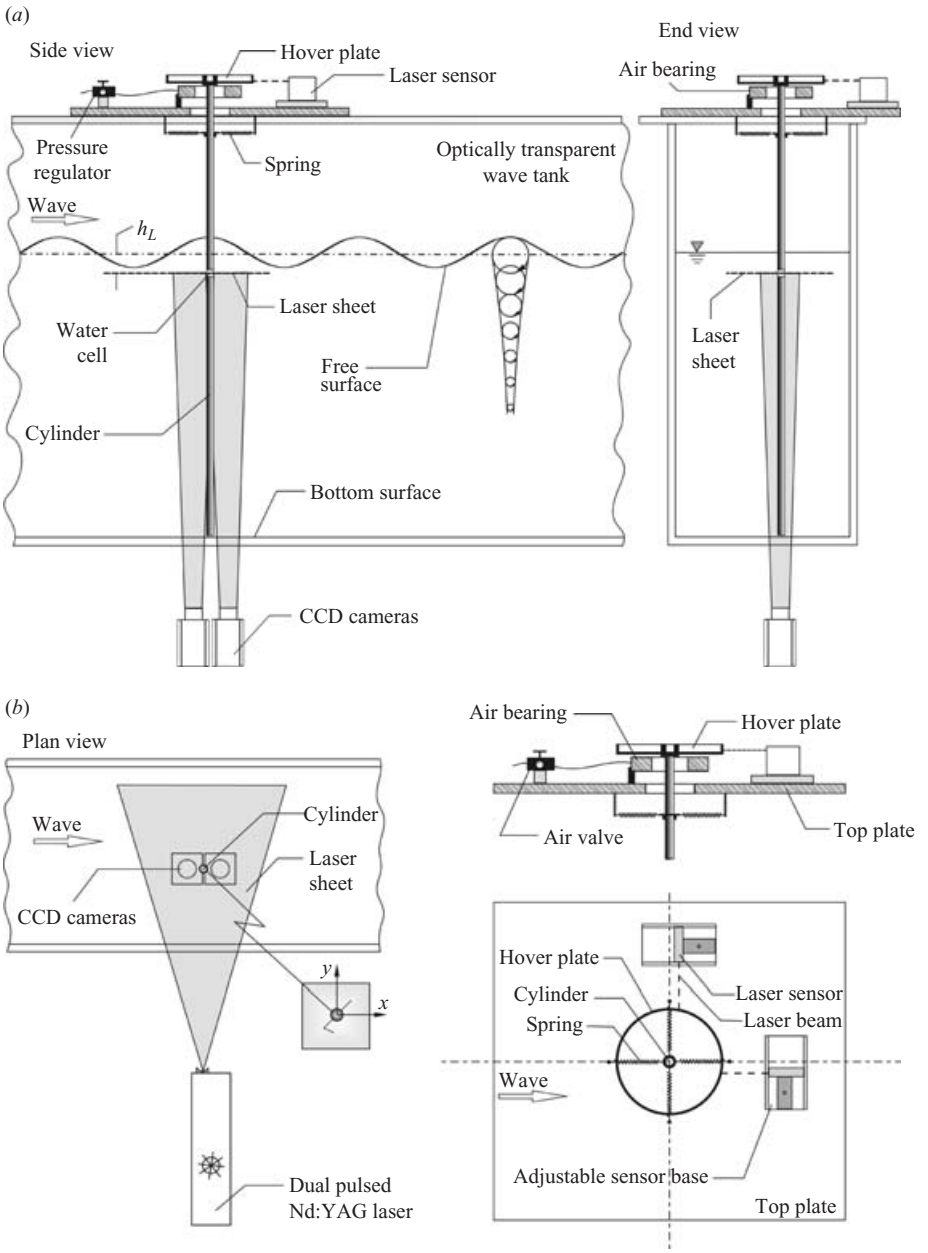

FIGURE 1. Schematic of the experimental facility for wave–structure interaction showing bidirectional elastic cylinder system, laser position sensor system, and laser illumination and image acquisition techniques.

2. Experimental system and techniques

2.1. *Wave tank–cylinder system*

Overviews of the experimental arrangement are given in figure 1. The wave tank had a depth of 1018 mm, a width of 426 mm and a total length of 9300 mm. Water was maintained at a level of 700 mm for all experiments. Waves of the desired frequency

and amplitude were generated using a paddle-type wave generator with actively controlled (forced) feedback, manufactured by Edinburgh Designs. The paddle is constructed in the form of a wedge-shaped aluminium paddle. A piezoelectric force transducer measures the load on the paddle and, via a feedback system, allows reflected energy to be reduced via impedance matching. An absorbent wedge system at the opposite end of the tank allowed, for the frequencies of interest in this investigation, insignificant wave reflection, when the force-feedback wave generator was employed.

For the present experiments, a value of wave frequency $f_w = 1.12$ Hz was employed. The wave amplitudes (half of the peak-to-peak amplitude of the wave motion) ranged from 2.82 mm to 24.54 mm. All generated waves were deep-water waves, as verified by independent quantitative imaging of the wave motion in the absence of the cylinder. The orbital trajectories of the wave were determined to be circular, with a radius that decreased exponentially with depth beneath the free surface. At a frequency of $f_w = 1.12$ Hz, corresponding to a wavelength $\lambda = 1.2$ m, the wave amplitude was 0.86 of its value at the free surface at an elevation of 30 mm beneath the free surface. The foregoing values of the wave frequency and wavelength, in conjunction with the cylinder diameter, satisfy the deep-water wave criteria defined in Sarpkaya & Isaacson (1981).

Vortex formation from the cylinder is a function of the Keulegan–Carpenter number $KC = U_w/f_w D$ in which f_w is the frequency of the wave, U_w is the peak velocity of the wave and D is the diameter for the cylinder. In addition, it is necessary to account for the Stokes number $\beta = f_w D^2/\nu = 404$, in which ν is kinematic viscosity; viscous diffusion can play a significant role in the evolution of patterns of vorticity. For the present experiments, the Reynolds number $Re = (KC)\,\beta = U_w D/\nu$ varied from 215 to 2491.

As indicated in figure 1, the vertical cylinder was mounted on an elastic system that allowed bidirectional motion. The cylinder was free to move in any direction in the horizontal plane, owing to circumferentially invariant stiffness. The total length of the cylinder was 1080 mm and the lengths of the submerged part of the cylinder were 695 mm and 700 mm, respectively, for the oscillating and stationary cylinder experiments. It had an outside diameter of 19 mm and a wall thickness of 0.25 mm. This very thin wall provided a low mass of the cylinder $m_c = 49$ g. The cylinder extended to the floor of the wave tank with a gap of less than 5 mm between the bottom end of the cylinder and the floor. This cylinder was rigidly attached to a hover plate made of lightweight Plexiglas material. The combined weight of the hover plate–cylinder arrangement was $m_c + m_H = 434$ g. The hover plate floated on top of an air-bearing system, which involved a doughnut-like chamber with 240 small holes of diameter 0.40 mm in its top surface. High-pressure air supplied to this chamber resulted in vertical oriented minijets that maintained the bottom surface of the hover plate at a distance of approximately 1 mm from the top surface of the air-bearing system. Regulated compressed air at a pressure of 40 p.s.i.g. was transmitted to the interior of a stationary annular air bearing. The cylinder was attached to a system of four springs (figure 1). Each of these springs was independently calibrated and verified to be linear over the range of deflection employed in the present experiment. The spring constant of each spring was $k = 0.011$ N mm^{-1}. These springs were attached to the cylinder with a small lightweight doughnut ring, which allows slipping between the cylinder and the spring system, thereby preventing the springs from producing a torsional load. Considering all of the foregoing components, the total effective mass m of the cylinder system was $m = 454$ g.

The natural frequency and logarithmic decrement of the free oscillation were determined from transient response experiments. These experiments showed that

the natural frequency in air was $f_{na} = 1.36\,\text{Hz}$ in both the x and y directions. The corresponding damping ratio was determined to be $\zeta_a = 0.0024$. The natural frequency in water is

$$f_{nw} = f_{na}\sqrt{\frac{m}{m + m_A}}, \tag{1}$$

in which $m_A = C_A^* m_d$. The hydrodynamic mass coefficient $C_A^* = 1$, and m_d is the mass of the displaced fluid. The values of m_A and f_{nw} are $m_A = 198\,\text{g}$ and $f_{nw} = 1.13\,\text{Hz}$ (in water) for both the x and y directions. The coefficient C_A^* should not be confused with the force coefficient that is in-phase with acceleration, typically determined from force measurements. The corresponding values of mass ratio and damping coefficient in water were determined using:

$$m^* = \frac{m}{m_d}, \tag{2}$$

$$\zeta_w = \zeta_a\sqrt{\frac{m}{m + m_A}}. \tag{3}$$

The values of these parameters were $m^* = 2.3$ and $\zeta_w = 0.00198$; therefore, $m^*\zeta_w = 0.0045$ for both the x and y directions. The present experiments focus on the case where the wave frequency f_w is equal to the natural frequency f_n of the cylinder system. This condition is satisfied within 0.8 %.

2.2. *Data acquisition system for bidirectional cylinder trajectory*

Laser sensors were employed to obtain the instantaneous cylinder displacements. Trajectories of the cylinder motion were measured using two sensors (figure 1). Sensor signals resulting from the motion of the cylinder never reached the limits of their corresponding sensing windows. Matlab software was used to calculate the cylinder coordinates.

The cylinder position was determined with the aid of trigonometric relations by using an in-house program, and the cylinder velocity was calculated from sequential cylinder positions on the processed image.

2.3. *Quantitative imaging systems*

A technique of digital particle image velocimetry (DPIV) was employed to characterize the instantaneous flow structure. Imaging was accomplished using a dual camera system, in conjunction with a laser sheet, both of which are shown in figure 1. The laser sheet was generated from a dual pulsed YAG system, having a maximum output of 90 mJ per pulse, which had time delays ranging from $\Delta t = 2\,\text{ms}$ to 9.5 ms for the present experiment. The water was seeded with 17.8 μm, metallic coated particles, which were essentially neutrally buoyant. A laser sheet of approximately 1.5 mm thickness at the location of the vertical cylinder was generated using a combination of spherical and cylindrical lenses at the head of the laser. This laser was located on a three-dimensional traverse system so that it could be precisely aligned relative to the cylinder. In order to ensure that the entire horizontal region about the cylinder could be illuminated, the laser sheet was transmitted through a water cell in the stainless steel cylinder at an elevation 30 mm below the mean surface level of the tank (figure 1*a*). This water cell involved a Plexiglas segment of the cylinder having the same diameter as the stainless steel cylinder and a wall thickness of 1.6 mm. It was filled with distilled water, and had a total length of 13 mm.

Two CCD cameras were located under the wave tank in order to accommodate the motion of the cylinder and to avoid obstructing the view owing to blockage

by the bottom of the cylinder (figure 1). The distance between the camera lenses was 85 mm. The cameras had a resolution of 1008 pixels × 1018 pixels. The distance from the camera lenses to the laser sheet location was 875 mm. Images on either side of the cylinder, acquired by the two cameras, were combined to provide a single overview image by using an in-house program. The last grid column of the left-hand side image and the first grid column of the right-hand side image were precisely overlapped during image acquisition. For all experiments, a value of magnification $M = 1:9.12$ was employed. This provided a field of view of 100 mm × 100 mm in the plane of the laser sheet. Patterns of particle images were acquired at a rate of 30 frames per second, thereby allowing 15 frame pairs per second. A frame-to-frame cross-correlation technique was employed to determine the velocity fields. The effective size of the interrogation window was 32 pixels × 32 pixels. The interrogation area contained approximately 15 to 25 particle images in order to satisfy the high-image density criterion. The effective grid size in the plane of the laser sheet, for both left-hand and right-right images, was 1.754 mm × 1.754 mm. In order to satisfy the Nyquist criterion, an overlap of 50 % was employed during the interrogation process. This procedure yielded a total of 6670 vectors for the combined frame. These patterns of velocity were, in turn, employed to construct instantaneous patterns of vorticity and the corresponding streamline topology. It was then possible to compare sequential images of the instantaneous flow structure at a given value of the KC number for either the stationary or oscillating cylinder.

In-house software was used to evaluate and remove inappropriate velocity vectors, caused by shadows, reflections, or laser sheet distortions in the flow field. A bilinear interpolation algorithm was then applied to the flow field without the invalid vectors. The field was then smoothed by a Gaussian weighted averaging technique. To minimize distortion of the velocity field, a smoothing parameter of 1.3 was chosen.

Time-averaging of the PIV data was accomplished with in-house software, which yielded mean (or time-averaged) values, root-mean-square (r.m.s.) values of velocity and vorticity, as well as the Reynolds stress correlations. Three images, at the same phase, were selected from the acquired sequence of 200 instantaneous images to obtain phase-averaged patterns for the cases of the stationary and oscillating cylinders. The intent of this type of averaging was to show the degree of deviation of representative instantaneous images.

The factors that contribute to uncertainty of velocity measured using the PIV technique are critically assessed by Adrian (1991), Raffel, Willert & Kompenhans (1998) and Westerweel (1993). The digital PIV (DPIV) approach employed herein is similar to that evaluated by Westerweel (1993); he concludes that an uncertainty of velocity within 2 % is an appropriate estimate.

3. Wave interaction with stationary cylinder: instantaneous patterns of vorticity and velocity

Patterns of instantaneous vorticity ω, velocity vectors $\boldsymbol{V}$ and normalized contours of constant streamwise $u^* = u/U_{max}$ and transverse (cross-stream) $v^* = v/U_{max}$ velocity components are given in figures 2 to 6 for a range of Keulegan–Carpenter number KC. The symbol U_{max} represents the maximum wave velocity at each value of KC. In all figures, N indicates the image number of a ciné sequence acquired during the wave period, which included 14 instantaneous PIV images, extending from $N = 1$ to $N = 14$. The image $N = 1$ corresponds to the instant at which the wave velocity has its maximum value in the direction of wave propagation.

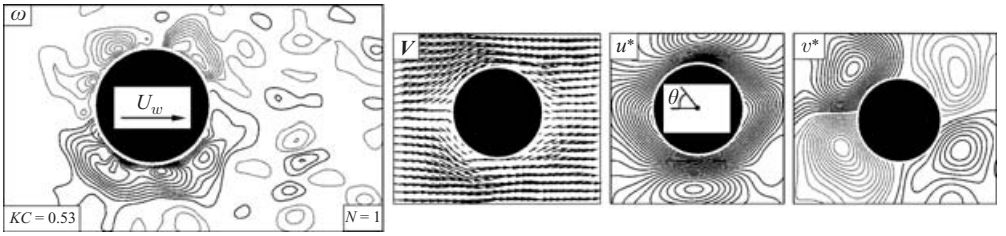

FIGURE 2. Patterns of instantaneous flow structure for a deep-water wave past a stationary cylinder at $KC = 0.53$. At instant $N = 1$, the instantaneous value of the wave velocity is at its maximum value of $U_w = 12.1\,\mathrm{mm\,s^{-1}}$. For instantaneous vorticity ω, $[\omega]_{min}$ and $\Delta[\omega]$ are both $0.3\,\mathrm{s^{-1}}$. For patterns of dimensionless instantaneous streamwise velocity component u^* and transverse component v^*, $[u^*]_{min} = [v*]_{min} = 0.05$ and $\Delta[u*] = \Delta[v*] = 0.025$.

3.1. *Symmetrical patterns without vortex shedding*

The images of figure 2, representing $KC = 0.53$, focus on the region near the surface of the cylinder. Image $N = 1$, which corresponds to the occurrence of the maximum velocity U_W of the wave motion, indicates the formation of positive and negative clusters of vorticity over the bottom and top surfaces of the cylinder. Furthermore, at this instant, very high magnitudes of streamwise velocity u^* are centred at $\theta = 90°$ and 270°. The patterns of v^* show, in an approximate sense, symmetry of the contours in each of four quadrants.

The pattern of vorticity clusters shown in $N = 1$ in figure 2 is generally similar to previously related investigations of sinusoidally oscillating flow past a fixed cylinder in the numerical simulations of Sun & Dalton (1996), Lin, Bearman & Graham (1996), and Tatsuno & Bearman (1990), as well as an oscillating cylinder in quiescent fluid visualized by Heinzer & Dalton (1969), all of which are for one-dimensional oscillatory motion, but at different combinations of KC and β.

Taken together, the images of figure 2, which are not associated with vortex shedding from the cylinder, provide a basis for interpretations at higher values of KC, as described in the following.

3.2. *Symmetrical patterns with shedding of small-scale vortices*

At $KC = 2.49$, as shown in figure 3, the instantaneous pattern of vorticity undergoes a fundamental change. Image $N = 1$ corresponds to the instant at which the wave velocity U_w has its maximum amplitude in the direction of wave propagation; this vector is indicated within the schematic of the cylinder at $N = 1$. For images $N = 2$ and 3, the magnitude of U_w is drawn to scale within the cylinder, thereby allowing cross-comparison of values of U_w with the maximum value occurring at $N = 1$. Furthermore, as indicated at the beginning of this section, the image sequence over one cycle of the wave oscillation extends from $N = 1$ to $N = 14$. Previously shed clusters of vorticity, arising during the preceding wave cycle, are evident; they are designated as A and C in images $N = 2$ and 3, and take the form of well-defined concentrations, with tails of relatively distributed vorticity extending over the right-hand portion of the image. Simultaneously, concentrations B and D become clearly defined in images $N = 2$ and 3, and at the left-hand side of the image, distributed tails of positive (solid line) and negative (dashed line) vorticity clusters persist.

Over this time span, corresponding to images $N = 1$ to 3 in figure 3, the patterns of u^* and v^* undergo substantial changes. At $N = 1$ and 2, u^* is positive everywhere, and at $N = 3$, negative pockets of u^* develop adjacent to the cylinder at $\theta = 0°$ and 180°.

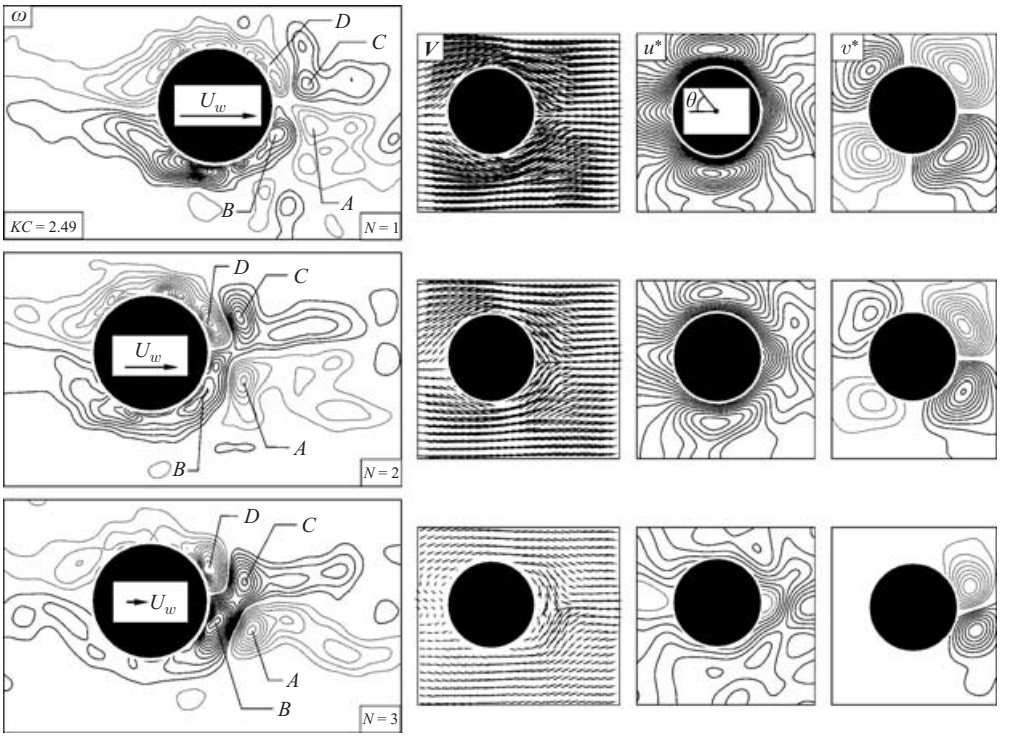

FIGURE 3. Patterns of instantaneous flow structure for a deep-water wave past a stationary cylinder at $KC = 2.49$. At instant $N = 1$, the instantaneous value of the wave velocity is at its maximum value of $U_w = 52.2\,\mathrm{mm\,s^{-1}}$. For instantaneous vorticity ω, $[\omega]_{min}$ and $\Delta[\omega]$ are both $0.75\,\mathrm{s^{-1}}$. For patterns of dimensionless streamwise velocity component u^*, $[u^*]_{min} = 0.025$ and $\Delta[u^*] = 0.05$. For instantaneous transverse componentv^*, $[v^*]_{min} = 0.075$ and $\Delta[v^*] = 0.05$.

Correspondingly, the pattern of v^* transforms from an approximately symmetrical structure in four quadrants to a significantly lower level of v^* over the left half of the cylinder, until at $N = 3$, significant levels of v^* occur only in the vicinity of $\theta = 180°$.

The pattern of vorticity at $N = 2$ in figure 3 is remarkably similar to that calculated numerically via a Floquet analysis by Elston, Sheridan & Blackburn (2004), at different values of KC and β. Furthermore, the numerical simulations of Sun & Dalton (1996), Guilmineu & Queutey (2002) and Dütsch *et al.* (1998) all show similar patterns at different combinations of KC and β. All of the foregoing investigations correspond to one-dimensional oscillatory conditions, so the strong agreement with the present results suggests that a sectional pattern of the flow structure owing to the oscillatory orbital wave motion interacting with the cylinder can be effectively interpreted via the pattern arising from one-dimensional motion.

3.3. *Nominally symmetric patterns with swept back vortices*

At $KC = 5.06$, represented in figure 4, the patterns of previously shed vorticity are swept back in the opposite direction past the cylinder and, as a consequence, lead to the remarkable pattern shown at $N = 1$. Concentrations C and A are from the previous cycle of the wave motion, while B and D are from the present cycle. At a later instant $N = 2$, a rightward direction of the wave motion results in, first of all, concentrations A and C moving away from the stack to the right. Simultaneously, concentration D is partitioned into a segment D' that moves with C, and a remaining segment

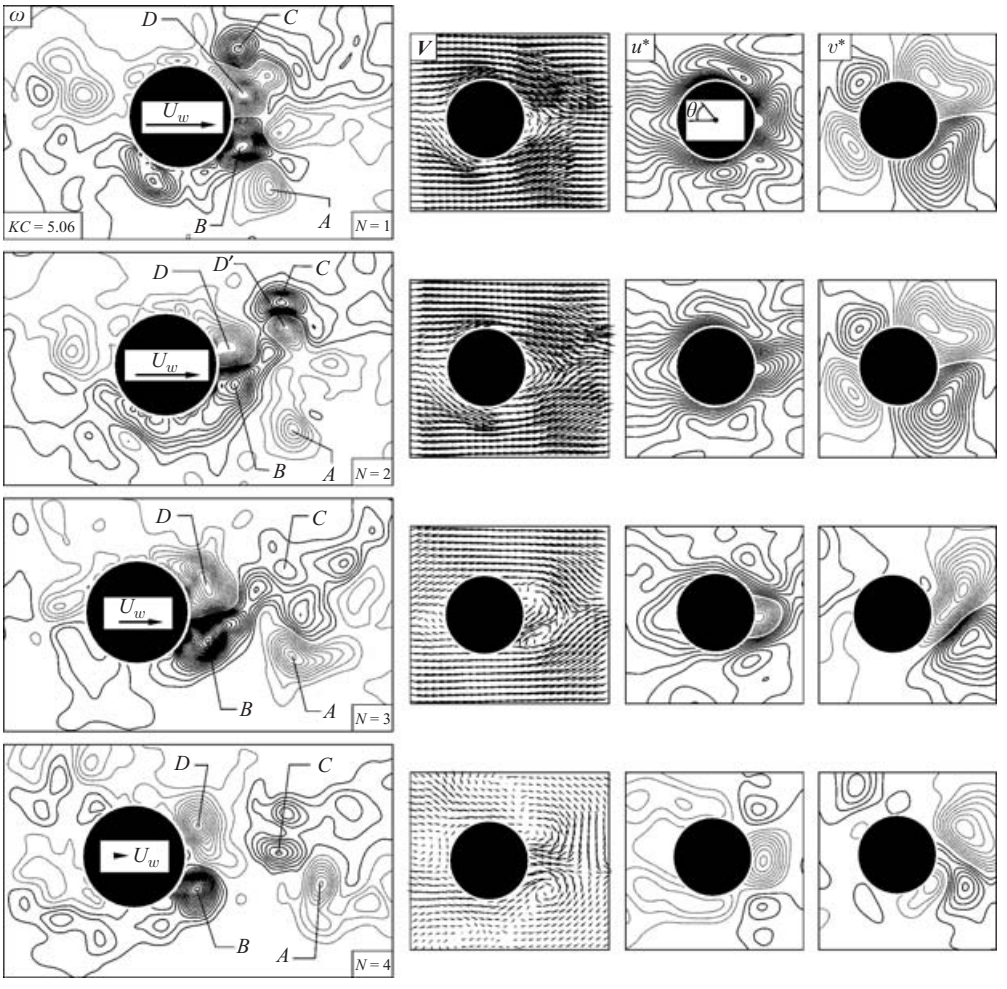

FIGURE 4. Patterns of instantaneous flow structure for a deep-water wave past a stationary cylinder at $KC = 5.06$. At instant $N = 1$, the instantaneous value of the wave velocity is at its maximum value of $U_w = 109.3\,\mathrm{mm\,s^{-1}}$. For instantaneous vorticity ω,$[\omega]_{min} = 1.5\,\mathrm{s^{-1}}$ and $\Delta[\omega] = 2\,\mathrm{s^{-1}}$. For patterns of dimensionless instantaneous streamwise velocity component u^* and transverse component v^*, $[u^*]_{min} = \Delta[u^*] = 0.075$ and $[v^*]_{min} = \Delta[v^*] = 0.05$.

D that remains adjacent to the cylinder. Continued development of this pattern of vorticity in image $N = 3$ shows that concentration D' is no longer detectable and broader distributions of the vorticity clusters A and C dominate that region, while in the vicinity of the cylinder, concentrations B and D have continued to accumulate vorticity, as well as experiencing an increase of peak vorticity level. As the wave velocity U_W tends to zero, indicated in $N = 4$, concentrations B and D move away from the plane of symmetry at $\theta = 180°$.

The corresponding patterns of u^* and v^* in figure 4 indicate substantial levels of positive u^* at instants $N = 1$ and 2, as well as high levels of v^* in each of the four quadrants. On the other hand, at instant $N = 3$, a negative pocket of u^* sets in at $\theta = 180°$ and, furthermore, the pattern of v^* on the right-hand side of the cylinder loses its symmetry. These general features persist at $N = 4$.

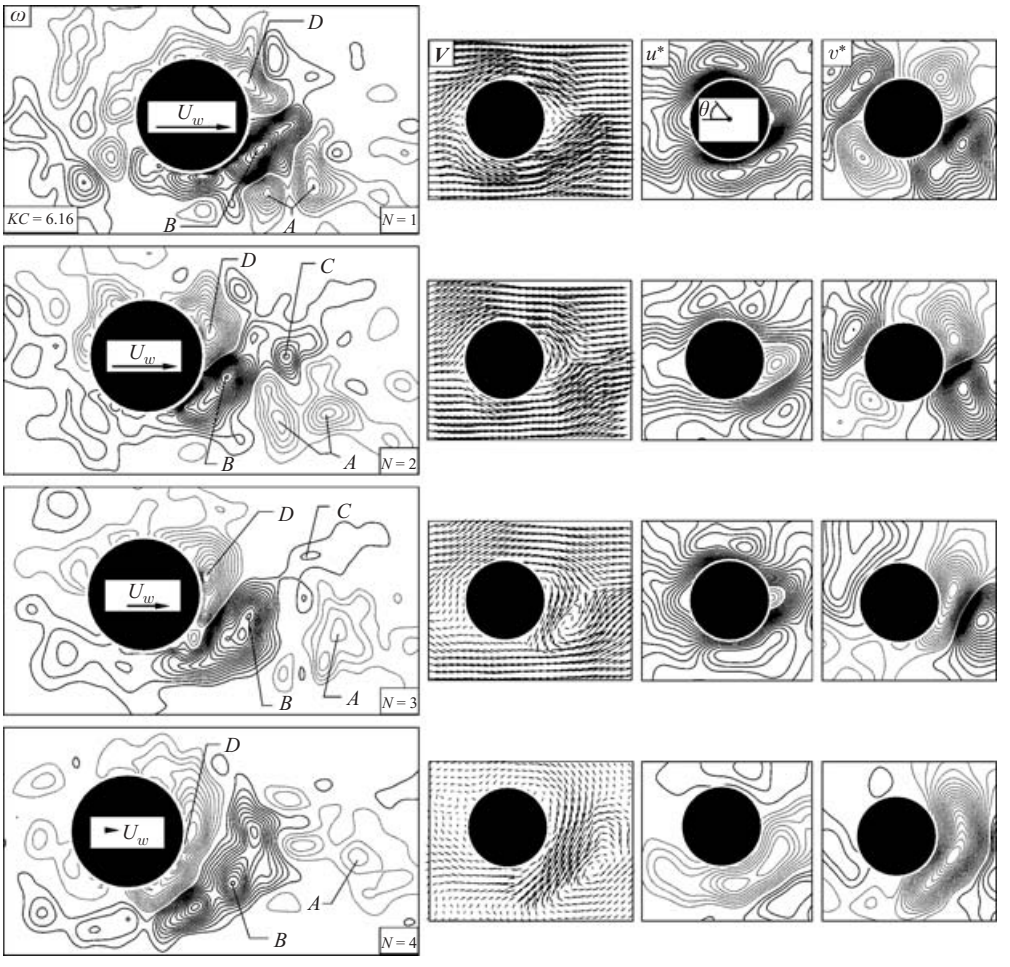

FIGURE 5. Patterns of instantaneous flow structure for a deep-water wave past a stationary cylinder at $KC = 6.16$. At instant $N = 1$, the instantaneous value of the wave velocity is at its maximum value of $U_w = 136.5\,\mathrm{mm\,s^{-1}}$. For instantaneous vorticity ω,$[\omega]_{min}$ and $\Delta[\omega]$ are both $3\,\mathrm{s^{-1}}$. For patterns of dimensionless instantaneous streamwise velocity component u^* and transverse component v^*, $[u^*]_{min} = \Delta[u^*] = 0.075$ and $[v^*]_{min} = \Delta[v^*] = 0.05$.

Experimental visualization by Williamson (1985*a*), using a marker technique in a one-dimensional oscillatory motion, indicates pairs of counter-rotating concentrations of vorticity, which are apparently directly analogous to the concentrations *A, B, C* and *D* indicated in image $N = 1$.

Note that the large-scale, elongated vortical structure *B* actually contains a number of small-scale embedded concentrations of vorticity, which are representative of the process of shear-layer transition. Comparison with previous images in the sequence shows that the large-scale concentration *B* does not contain small-scale concentrations, thereby indicating that the occurrence of transition phenomena in the separating shear layer may occur only over a limited portion of the wave cycle.

3.4. *Onset of asymmetrical large-scale vortex formation*

At the value of $KC = 6.16$ shown in figure 5, image $N = 1$ shows pre-existing clusters of vorticity *A* shed during a previous wave cycle; they have moved past the cylinder

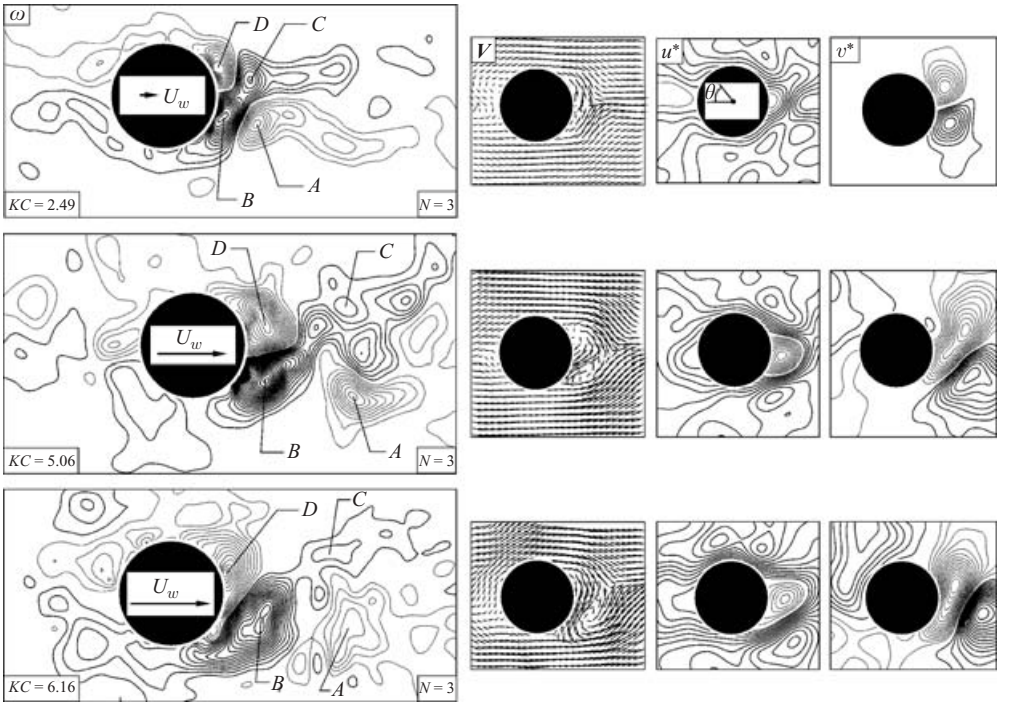

FIGURE 6. Comparison of instantaneous patterns at the same instant of wave cycle for values of $KC = 2.49$, 5.06 and 6.16. For all KC, values of minimum and incremental vorticity of dimensionless streamwise velocity component u^* and dimensionless transverse velocity component v^* are the same as indicated in the captions of figures 3 to 5. For purposes of reference, the magnitude of the instantaneous wave velocity is $U_w = 74.1\,\mathrm{mm\,s^{-1}}$ at $N = 3$ for $KC = 6.16$.

to the opposite side. The mirror image of this pattern of vorticity does not exist on the opposite side of the wake. Clusters B and D are in the process of formation during the present wave cycle. In subsequent images, $N = 2$ and 3, concentrations B and D develop further with an increasing level of asymmetry and, finally, in image $N = 4$, elongated vorticity layers B and D tend to form a Kármán-like street, together with cluster A. Moreover, the negative vorticity cluster D extends over a larger portion of the cylinder surface as the wave velocity decreases.

The corresponding pattern of velocity vectors $\boldsymbol{V}$ of figure 5 indicates that the foregoing process is associated with formation of a downward directed jet, of increasing spatial extent and intensity, in images $N = 2$ to 4. Correspondingly, the patterns of dimensionless vertical velocity v^* transform from a roughly symmetrical pattern in image $N = 1$, with high levels of v^* in each quadrant, to a pattern that is nearly dominated by a high level of downward directed v^* in image $N = 4$. This process is accompanied by transformations of the patterns of u^*, involving the onset of a negative pocket of $u^* = 180^\circ$ at $N = 2$, and eventually a predominant elongated region of negative u^* at $N = 4$.

Figure 6 gives a direct comparison of the patterns of vorticity at the same phase of the wave cycle ($N = 3$) for different values of $KC = 2.49$, 5.06 and 6.16. At all values of KC, a positive vorticity layer extends from the bottom surface of the cylinder to the upper side of the near wake. The relevant concentrations of vorticity are B and C. This extension of the positive layer across the wake, in effect, partitions the negative

concentrations A and D. With increasing KC, the scale of concentration B increases and the distance between the negative concentrations A and D increases as well.

Located immediately adjacent to each pattern of vorticity in figure 6 is the pattern of instantaneous velocity vectors $\boldsymbol{V}$. This pattern covers the right-hand part of each vorticity image and thereby potentially reveals localized swirl patterns of velocity vectors that would represent the vorticity concentrations. It is evident, however, upon inspection of these patterns, that only certain of the concentrations A to D defined in the patterns of vorticity are suggested in the patterns of velocity. Regarding the patterns of u^* shown in the third column of figure 6, it is evident that an increase in the value of KC yields a pocket of negative streamwise velocity at sufficiently high values of $KC = 5.06$ and 6.16; the very initial stages of formation of this pocket are, however, evident in the u^* image at $KC = 2.49$. As for the patterns of v^*, they become severely asymmetrical in the wake region at $KC = 5.06$ and 6.16, relative to approximately symmetrical patterns at $KC = 2.49$. This increased asymmetry is associated with a tendency towards formation of large-scale vortical structures in the near wake, evident from the patterns of vorticity at $KC = 5.06$ and 6.16.

Viewing together figures 3 to 6, in particular the patterns of instantaneous streamwise velocity u^*, it is evident that pockets of negative (dashed line) u^* can occur. In figure 3, for the relatively low value of $KC = 2.49$, such a negative pocket is distinguishable only at the phase of the wave motion corresponding to $N = 3$, while at larger values of $KC = 5.06$ and 6.16 in figures 4 and 5, respectively, these negative pockets of u^* can occur over a wider range of phase of the wave motion, i.e. at $N = 3$ and 4 in figure 4 and $N = 2$ and 3 in figure 5. Generally speaking, these pockets or clusters of negative u^* immediately adjacent to the surface of the cylinder are an indication of the extent of the separation bubble. It is evident that its existence and scale can vary dramatically over the wave cycle.

Figure 7 shows a comparison of instantaneous (left-hand column) and phase-averaged (right-hand column) patterns of vorticity, designated, respectively, as ω and $\langle\omega\rangle_p$. These phase-averaged patterns were determined using the approach described in § 2. It is evident that the predominant features of the patterns of ω and $\langle\omega\rangle_p$ are closely correlated, thereby reaffirming the use of instantaneous patterns as representations of the flow physics.

4. Wave interaction with a stationary cylinder: steady-state patterns

The oscillatory wave motion past the cylinder is associated with an underlying, steady-state pattern of vorticity. Figure 8 shows patterns of averaged vorticity $\langle\omega\rangle$ for the range of KC addressed herein. At the lowest value of $KC = 0.53$, ordered patterns of $\langle\omega\rangle$ were not clearly evident; therefore, this KC is not represented in figure 8. At $KC = 2.49$, small-scale concentrations at the surface of the cylinder are bounded by relatively large-scale, elongated clusters of opposite vorticity. These clusters contain a vorticity concentration in the region close to the surface of the cylinder, and show decreasing levels of essentially distributed vorticity away from the cylinder surface. At $KC = 5.06$, the clusters of vorticity adjacent to the cylinder surface show a substantial increase in scale and level of peak vorticity. Such concentrations are also bounded by regions of vorticity of opposite sign that extend a significant distance away from the surface of the cylinder. These outer clusters of vorticity have a substantially reduced level of peak vorticity, relative to the outer clusters at $KC = 2.49$. Moreover, the clusters at $KC = 5.06$ are distributed over a region of significantly larger extent. Finally, at $KC = 6.16$, the concentrations of vorticity immediately adjacent to the

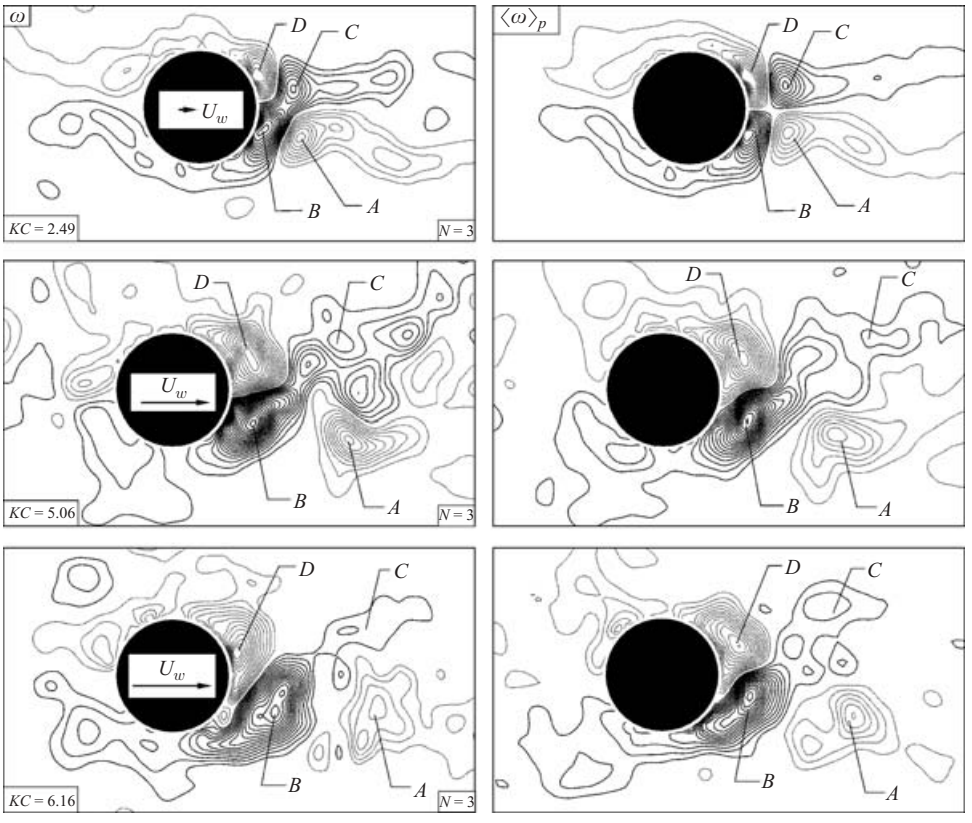

FIGURE 7. Comparison of instantaneous (left column) and phase-averaged patterns (right column) of vorticity. Minimum and incremental values at each value of KC are the same as given in figures 3 to 5. For purposes of reference, magnitude of instantaneous wave velocity is $U_w = 74.1\,\mathrm{mm\,s^{-1}}$ at $N = 3$ for $KC = 6.16$.

cylinder have a somewhat larger spatial extent and higher peak vorticity values than those at 5.06. The clusters of vorticity in the outer region away from the cylinder are, however, less well defined than at lower values of KC.

Patterns of root-mean-square vorticity ω_{rms} are given in the middle column of figure 8. The common feature, over the entire range of KC, is four identifiable clusters, or concentrations, of ω_{rms}, which are distributed over the four quadrants. At low KC, they tend to appear roughly near the centre of each quadrant, and for increasing KC, move closer to $\theta = 0°$ and 180°.

Patterns of the Reynolds stress correlation $\langle u'v' \rangle / U_m^2$ are given in the right-hand column of figure 8. Defined contours extend well away from the surface of the cylinder, and the spatial extent of each of these contours significantly exceeds the extent of the vorticity concentrations adjacent to the surface of the cylinder.

5. Self-excited oscillations of the cylinder due to wave interaction: trajectories

If the cylinder is not held in a stationary position, but allowed to undergo self-excited vibrations, several types of trajectory are generated. A basic form of trajectory is an ellipse inclined with respect to the direction of the wave motion. The build-up from the cylinder at rest to the steady-state limit cycle of the oscillation is

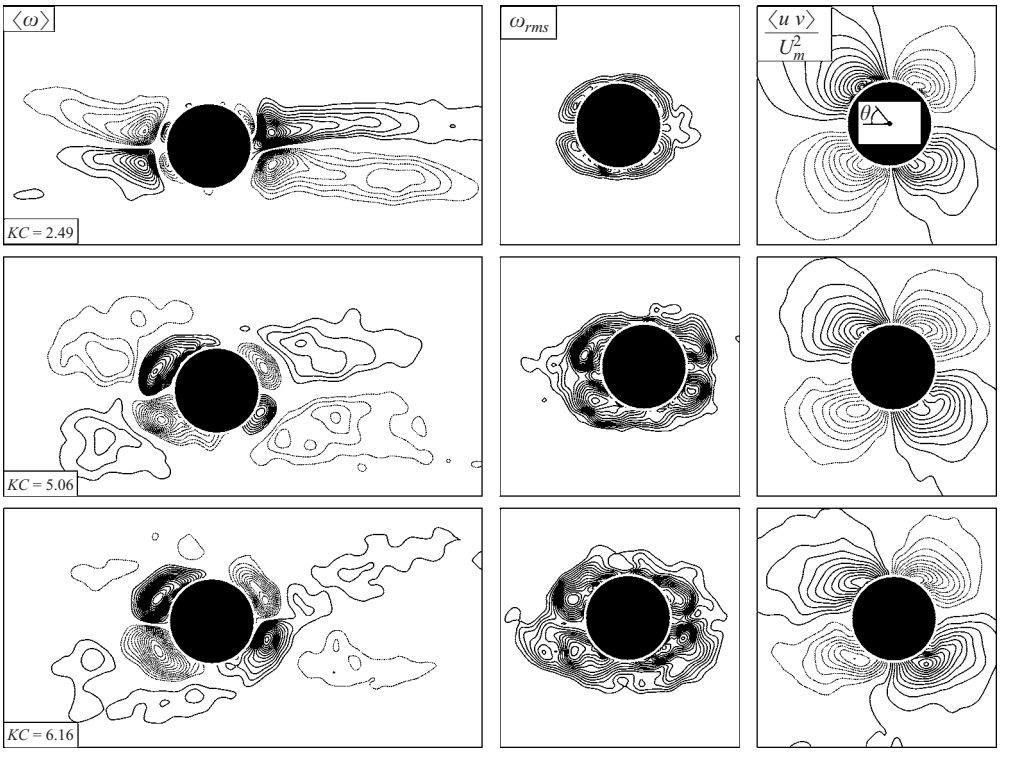

FIGURE 8. Patterns of time-averaged vorticity $\langle\omega\rangle$, root-mean-square vorticity ω_{rms} and averaged Reynolds stress correlation $\langle u'v'\rangle/U_m^2$ for indicated values of KC. For instantaneous vorticity ω, at $KC = 2.49$, 5.06 and 6.16, respective values of $[\langle\omega\rangle]_n = 0.4$, 1.0 and $1\,\mathrm{s}^{-1}$ and $\Delta[\langle\omega\rangle] = 0.2$, 0.5 and $0.75\,\mathrm{s}^{-1}$. For root-mean-square vorticity ω_{rms}, at $KC = 2.49$, 5.06 and 6.16, respective values of $[\omega_{rms}]_{min} = 1.5$, 4 and $6\,\mathrm{s}^{-1}$ and $\Delta[\omega_{rms}] = 0.5$, 0.75 and $1.0\,\mathrm{s}^{-1}$. For Reynolds stress correlation $\langle u'v'\rangle/U_m^2$, at all values of KC, $[\langle u'v'\rangle/U_m^2]_{min}$ and $\Delta[\langle u'v'\rangle/U_m^2]$ are both 0.025.

shown in figure 9(*a*). Figure 9(*a*) (i) shows approximately the first seven cycles of oscillation, which results in a sequence of nearly horizontal, highly elongated ellipses. They eventually culminate in an ellipse that has a peak amplitude of nearly $0.2D$. Figure 9(*a*)(ii) shows not only the initial trajectories (figure 9*a*(i)), but also the sequence that leads to the eventual limit-cycle oscillation. As indicated, the elongated, nearly horizontal elliptical trajectory of figure 9(a)(i) rotates, and becomes wider, until the limit cycle is attained. This limit cycle, which is shown in figure 9(*a*)(iii), corresponds to approximately 120 wave cycles.

Figure 9(*b*) provides an overview of the steady-state oscillation cycles for the range of KC considered herein. At the lowest values of $KC = 0.53$ and 2.49, approximately elliptical forms of trajectories are generated. At $KC = 2.49$, however, a second admissible trajectory is attainable, depending upon the initial conditions and history of development during the build-up phase of the oscillation. This cycle is nearly in-line. Furthermore, a predominantly in-line pattern occurs at $KC = 5.06$. For the highest value of $KC = 6.16$, the pattern suggests a figure-of-eight trajectory.

Figure 9(*c*) shows the limit-cycle trajectories over approximately the last two cycles of oscillation. The trajectories at $KC = 0.53$ and 2.49 are represented well by the steady-state limit cycles of figure 9(*b*), extending over 120 cycles. At $KC = 2.49$, as well

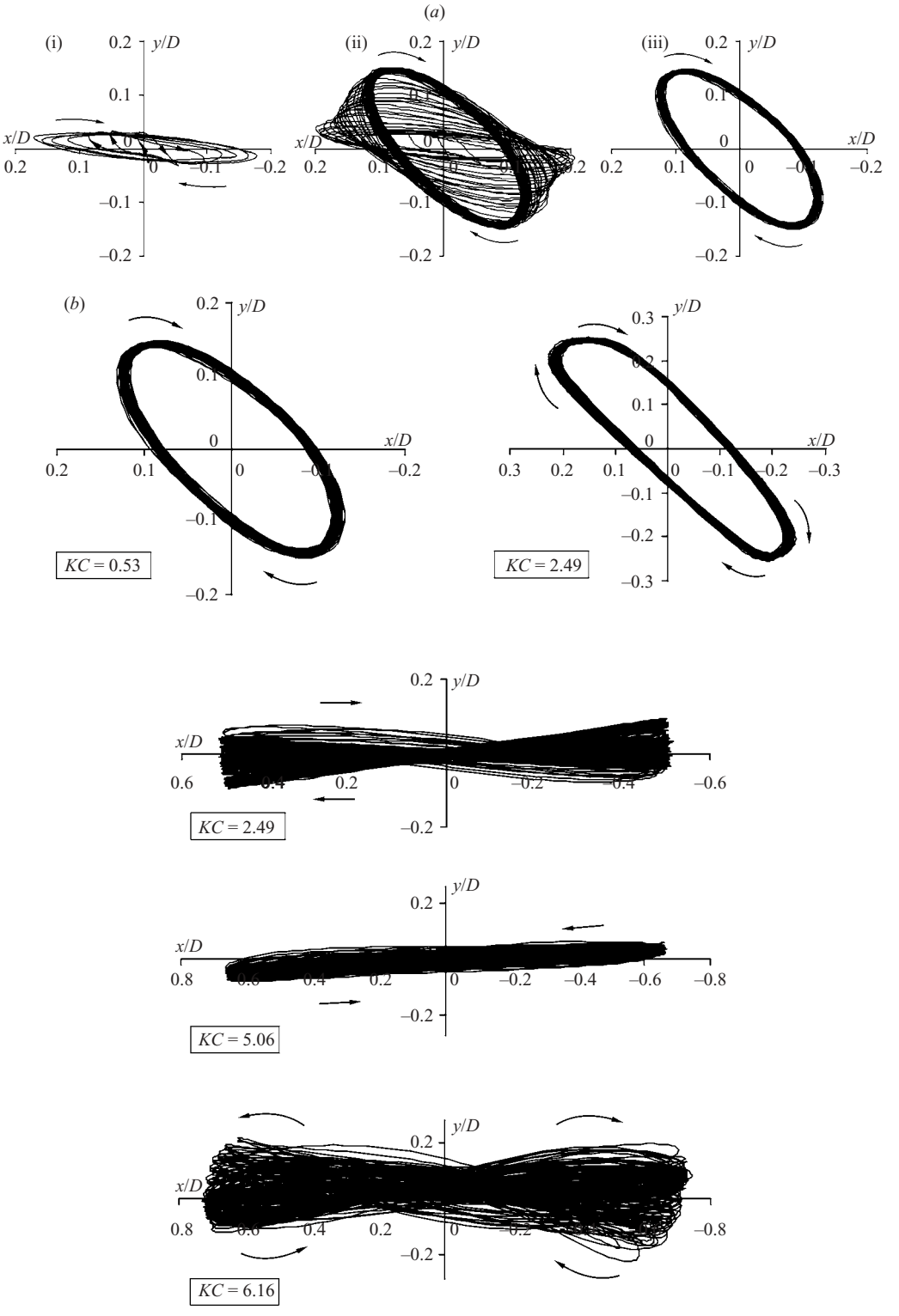

FIGURE 9(*a*,*b*). For caption see facing page.

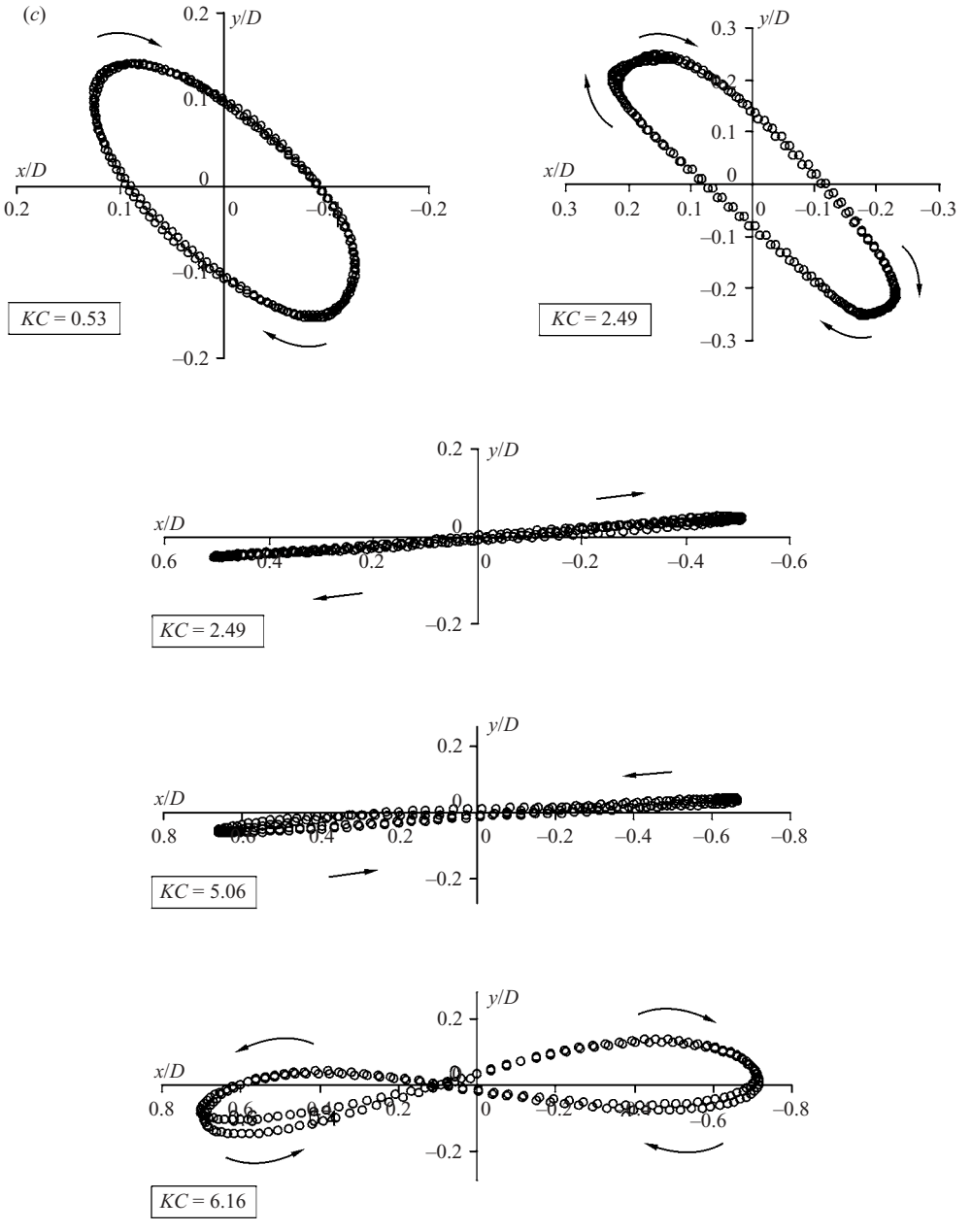

FIGURE 9. (*a*) Onset of the elliptical limit-cycle trajectory of an elastically mounted cylinder in a deep-water wave: (i) first seven cycles of oscillation starting from cylinder rest; (ii) trajectories of oscillation cycles starting from rest to attainment of steady-state elliptical limit cycle; and (iii) steady-state limit cycle corresponding to superposition of approximately 120 cycles. $KC = 0.53$. (*b*) Steady-state limit-cycle trajectories for indicated values of KC. For all values of KC, a total of approximately 120 oscillation cycles are indicated. (*c*) Limit-cycle trajectories showing the final two cycles of oscillation for indicated values of KC.

as $KC = 5.06$, the trajectories of figure 9(*c*) are nearly aligned with the x-axis. At $KC = 6.16$, a figure-of-eight trajectory is clearly evident. It is evident that the patterns of figure 9(*b*), for values of $KC = 2.49$, 5.06 and 6.16, incorporate modulations of the

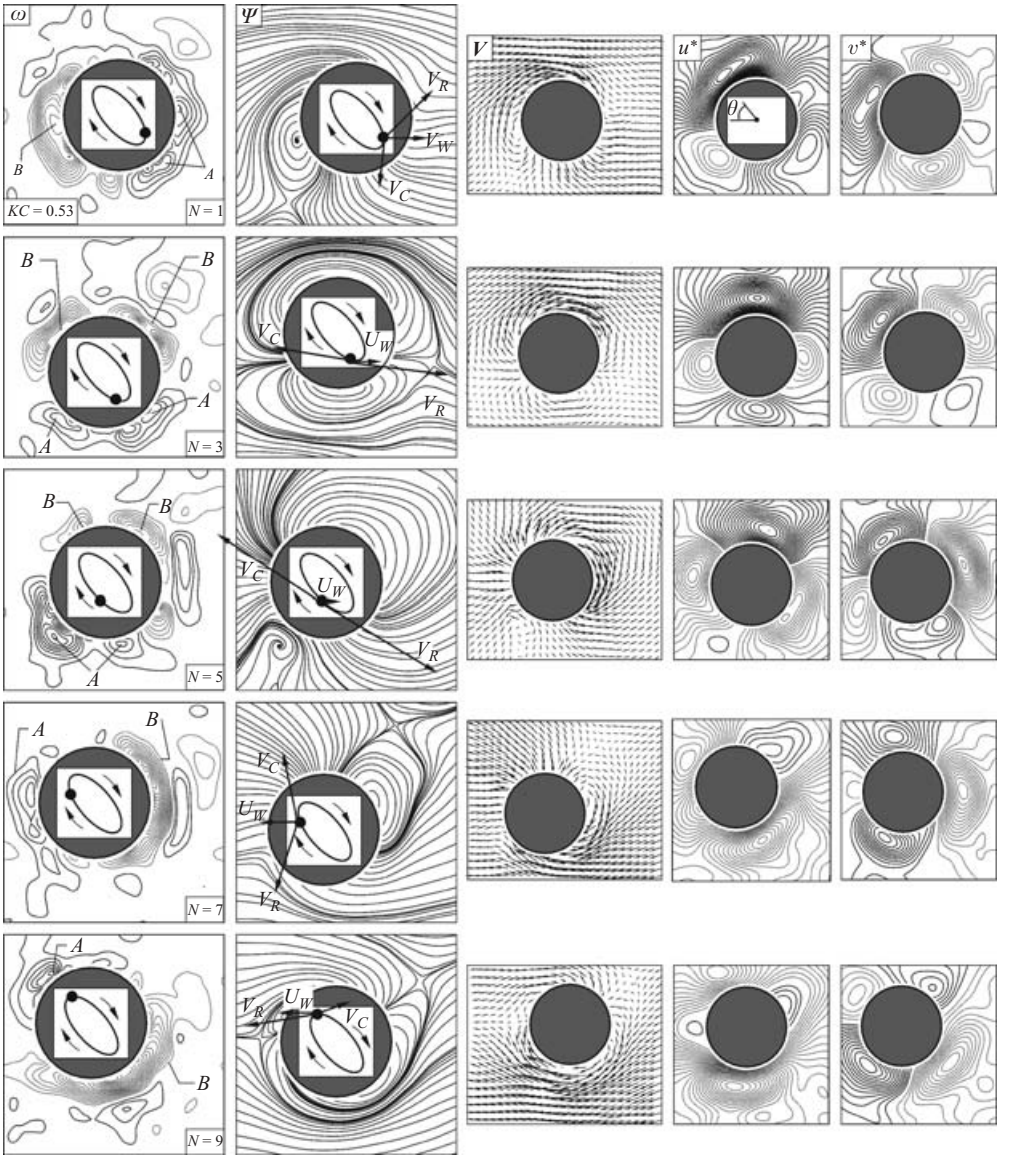

FIGURE 10. Patterns of instantaneous flow structure during the oscillation cycle of a cylinder at $KC = 0.53$. At instant $N = 1$, the instantaneous value of the wave velocity is at its maximum value of $U_w = 11.5\,\mathrm{mm\,s^{-1}}$. For instantaneous vorticity ω,$[\omega]_{min}$ and $\Delta[\omega]$ are both $0.6\,\mathrm{s^{-1}}$. For patterns of dimensionless instantaneous streamwise velocity component u^* and transverse component v^*, $[u^*]_{min} = [v^*]_{min} = \Delta[u^*] = \Delta[v^*] = 0.1$.

limit-cycle trajectories about the relatively well-defined end-state trajectories given in figure 9(*c*).

6. Self-excited oscillations of the cylinder owing to wave interaction: patterns of flow structure in relation to the trajectory and relative velocity of the wave

6.1. *Elliptical trajectory of cylinder*

Figure 10 shows, for $KC = 0.53$, patterns of instantaneous vorticity ω, streamline ψ topology and total velocity vectors $\boldsymbol{V}$, as well as the dimensionless velocity components

u^* and v^*. The elliptical trajectory is represented at the interior of each cylinder, and the instantaneous position of the cylinder is designated by a black dot. On the images of streamline ψ topology, the instantaneous velocity U_W of the wave, the cylinder velocity V_C, and the relative velocity V_R of the wave with respect to the cylinder are indicated for each instantaneous position of the cylinder.

Consider, first of all, the patterns of instantaneous vorticity. By examining the sequence $N=1$ to $N=9$, it is evident that, as the cylinder moves around its elliptical trajectory, the layers of vorticity A and B adjacent to the cylinder surface rotate about the cylinder. Although these layers A and B remain predominantly distributed, pronounced concentrations of vorticity are evident at certain instants during the wave cycle. For example, at $N=3$, layer A can be considered to involve two subconcentrations designated as A, and likewise for layer B.

If we consider the patterns of instantaneous streamline ψ topology, as given in the second column of figure 10, severe transformations occur for successive values of N. By directly comparing the patterns of ψ with the velocity vectors $\boldsymbol{V}$, given in the third column, it is possible to see that a well-defined bubble exists at all values of N. This bubble involves streamlines that are initially oriented away from the cylinder surface, then towards the surface. It should be emphasized that each of these streamlines does not necessarily indicate a process of separation, followed by reattachment. Rather, the streamline pattern within the bubble, which is dependent upon the reference frame, serves as a guide for interpretation of the patterns of vorticity layers that rotate around the periphery of the cylinder. At $N=1$, this bubble extends over the portion of the cylinder surface from approximately $\theta=310^\circ$ to 33°; θ is defined in the top row of images. Then, at larger values of $N=3$, 5, 7 and 9, it extends over the following values of θ : $340^\circ \leqslant \theta \leqslant 215^\circ$; $37^\circ \leqslant \theta \leqslant 215^\circ$; $107^\circ \leqslant \theta \leqslant 205^\circ$; and $145^\circ \leqslant \theta \leqslant 10^\circ$. This bubble therefore rotates about the surface of the cylinder as it moves on its elliptical trajectory. At any given instant N, it is generally coincident with the central region of the negative layer of vorticity B. Furthermore, an additional bubble is evident at instant $N=3$. It extends over $215^\circ \leqslant \theta \leqslant 322^\circ$, and is generally coincident with the positive layer of vorticity A. While the instantaneous velocity U_W of the wave is smallest at $N=5$, the cylinder velocity V_C and the relative velocity V_R of the wave with respect to the cylinder have taken their maximum values. The development of these bubble patterns is associated with the patterns of u^* and v^* given in the fourth and fifth columns of figure 10.

At a larger value of $KC=2.49$, the flow structure takes the form shown in figure 11. As the cylinder moves about its elliptical trajectory, the patterns of vorticity rotate about the surface of the cylinder. Vorticity layer C rotates to an angle of approximately 180° in images $N=2$ to 10. On the other hand, layer D, which is clearly defined at $N=2$ and 4, departs from the surface of the cylinder at $N=6$ and rapidly degenerates at subsequent instants. Vorticity clusters A and B, which were formed earlier and have departed from the surface of the cylinder, appear at the outer boundary of layer C in images $N=2$, 4 and 6, 2 to 8; in essence, they rotate about the cylinder with concentration C. The distinguishing feature of the patterns of vorticity at this value of $KC=2.49$, relative to those at $KC=0.53$ in figure 10, is the persistence of previously shed layers of vorticity exterior to those immediately adjacent to the surface of the cylinder. If we consider image $N=8$ in figure 11, it is possible to discern four layers of vorticity in the lower right-hand region of the image, starting with C along the surface, then A, followed by two other unmarked layers.

Patterns of streamline topology, in figure 11, indicate the existence of a separation bubble in the plots of ψ, whose interpretation is aided with the patterns of $\boldsymbol{V}$ at instants $N=4$, 6 and 10. A high degree of correlation exists between the angular

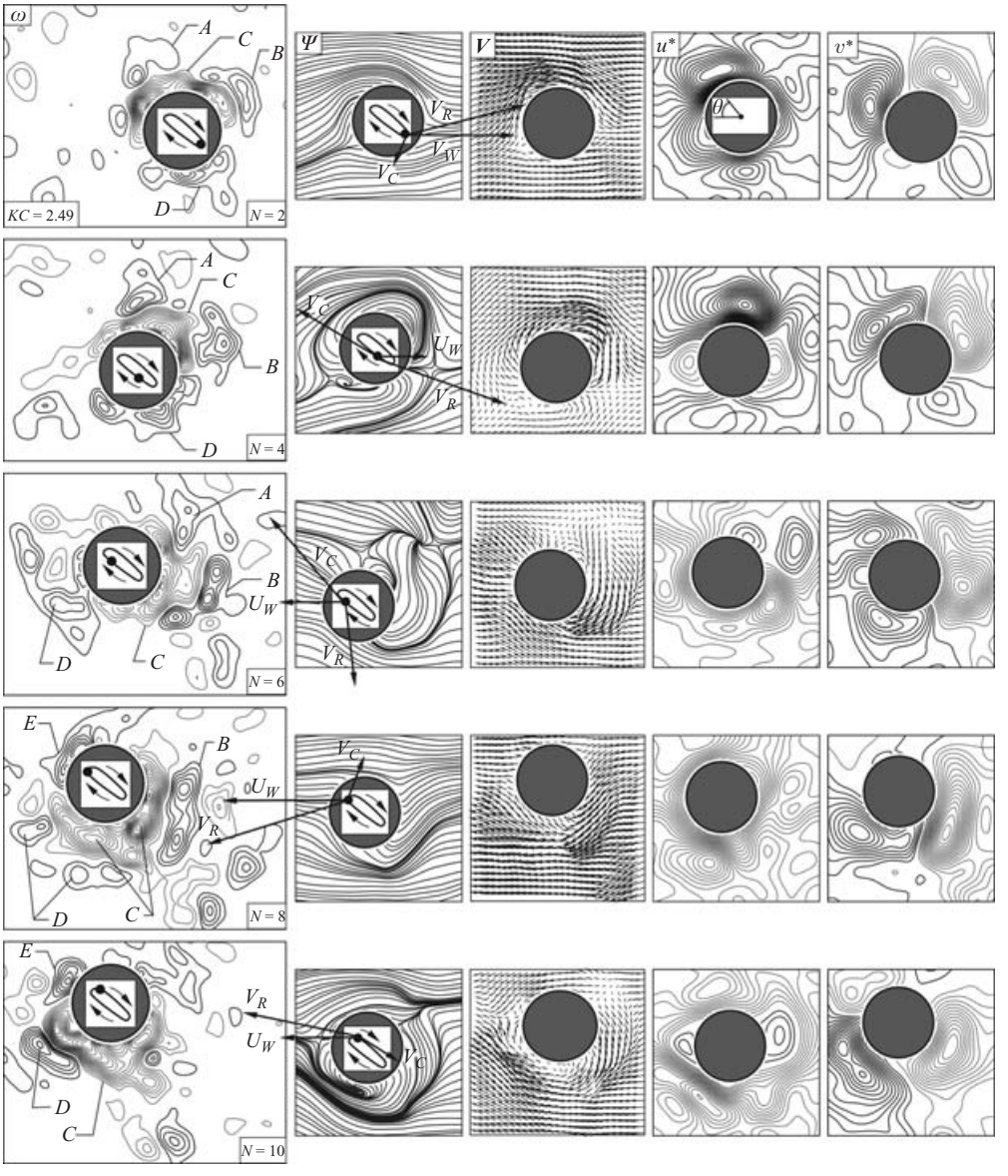

FIGURE 11. Patterns of instantaneous flow structure during the oscillation cycle of a cylinder at $KC = 2.49$. At $N = 2$, the magnitude of the instantaneous wave velocity is $U_w = 49.6\,\mathrm{mm\,s^{-1}}$. For instantaneous vorticity ω,$[\omega]_{min}$ and $\Delta[\omega]$ are both $1.5\,\mathrm{s^{-1}}$. For patterns of dimensionless instantaneous streamwise velocity component u^* and transverse component v^*, $[u^*]_{min} = [v^*]_{min} = \Delta[u^*] = \Delta[v^*] = 0.075$.

positions of the large-scale streamline bubble on the cylinder surface and the relative velocity vector V_R; both rotate sequentially in successive images by approximately the angular displacement. In turn, the streamline bubble rotation is in accord with the rotation of the corresponding vorticity layer about the cylinder surface. This bubble rotates about the cylinder in accord with the vorticity layer C. Patterns of the velocity components u^* and v^* are severely distorted with increasing values of N, in accord with the rotation of the bubble-like pattern about the surface of the

cylinder. Extrema (peak values) of clusters of u^* contours adjacent to the surface of the cylinder generally define the central portions of the aforementioned vorticity layers and streamline bubbles along the surface. That is, at $N = 2$ and 4, the extrema of positive (solid line) contours are evident along the upper surface of the cylinder, and at $N = 6$ to 10, where the contours take on negative values, the positions of the extrema rotate towards the bottom surface of the cylinder, and continue to track the centres of the bubbles and the vorticity layers.

6.2. *In-line trajectory*

At $KC = 2.49$, an alternative trajectory in the form of a nearly in-line oscillation is attainable, as indicated in figure 3. The detailed flow structure associated with this essentially in-line motion is given in figure 12. Regarding the patterns of vorticity, at $N = 2$, concentrations B and C form from the cylinder, and at $N = 4$, these concentrations form a stack-like arrangement involving A, B, C and D. At this instant, the relative wave velocity V_R is nearly maximum to the right-hand side. This stacked pattern is remarkably similar to that from the stationary cylinder, shown in image $N = 1$ in figure 4, for which $KC = 5.06$. Furthermore, the computational results of one-dimensional oscillating flow past a fixed circular cylinder of Zhang & Dalton (1999) display a similar pattern at different values of KC and β.

The combination of the wave velocity U_W and cylinder velocity V_C apparently yield a higher effective value of V_R, for purposes of vortex formation, than that based solely on the maximum amplitude of the wave velocity U_W. Furthermore, the vorticity pattern at $N = 6$ in figure 12 broadly resembles that at $N = 2$ in figure 4. That is, concentrations B and C continue to develop adjacent to the base of the cylinder, while previously shed concentrations A and D move away from the cylinder, i.e. depart from the ends of the stacked arrangement. In the meantime, vorticity clusters E and F persist at the left-hand side of the cylinder. At later instants of time $N = 8$, 10, the direction of the relative wave velocity V_R reverses and the formation of new concentrations of vorticity G and H commence.

Regarding the patterns of streamline ψ topology in figure 12, when separation bubbles form, they appear to do so in an approximately symmetrical fashion, as indicated in the ψ patterns of images $N = 4$ and $N = 10$ in figure 12. These bubble patterns form when the magnitude of the relative wave velocity V_R approximately attains its maximum value.

Such bubble patterns are consistent with pronounced layers of vorticity over the upper and lower surfaces of the cylinder at $N = 4$ and 10. Concerning the patterns of u^* and v^*, contours of these quantities are partitioned in the four quadrants and tend to show mirror image patterns with respect to either a horizontal or vertical reference line, the variation in peak values of sets of contours of u^* and v^* not withstanding. At all of the values of N in the series of figure 12, this is not the case.

At a higher value of $KC = 5.06$, represented in figure 13, we again see the formation of a stacked arrangement of vorticity concentrations A, B, C and D at instant $N = 2$, which approximately corresponds to the maximum relative wave velocity V_R. This pattern is generally similar to that at $N = 4$ in figure 12. At a later instant, the stacked arrangement transforms to a pattern involving asymmetrical clusters B and C from the surface of the cylinder, while D departs to the right.

The corresponding pattern of streamline ψ topology in figure 13 indicates bubble-like regions on the lower and upper surfaces of the cylinder, though by simultaneously considering the velocity field $\boldsymbol{V}$ at $N = 4$ and $N = 10$, the bubble pattern is

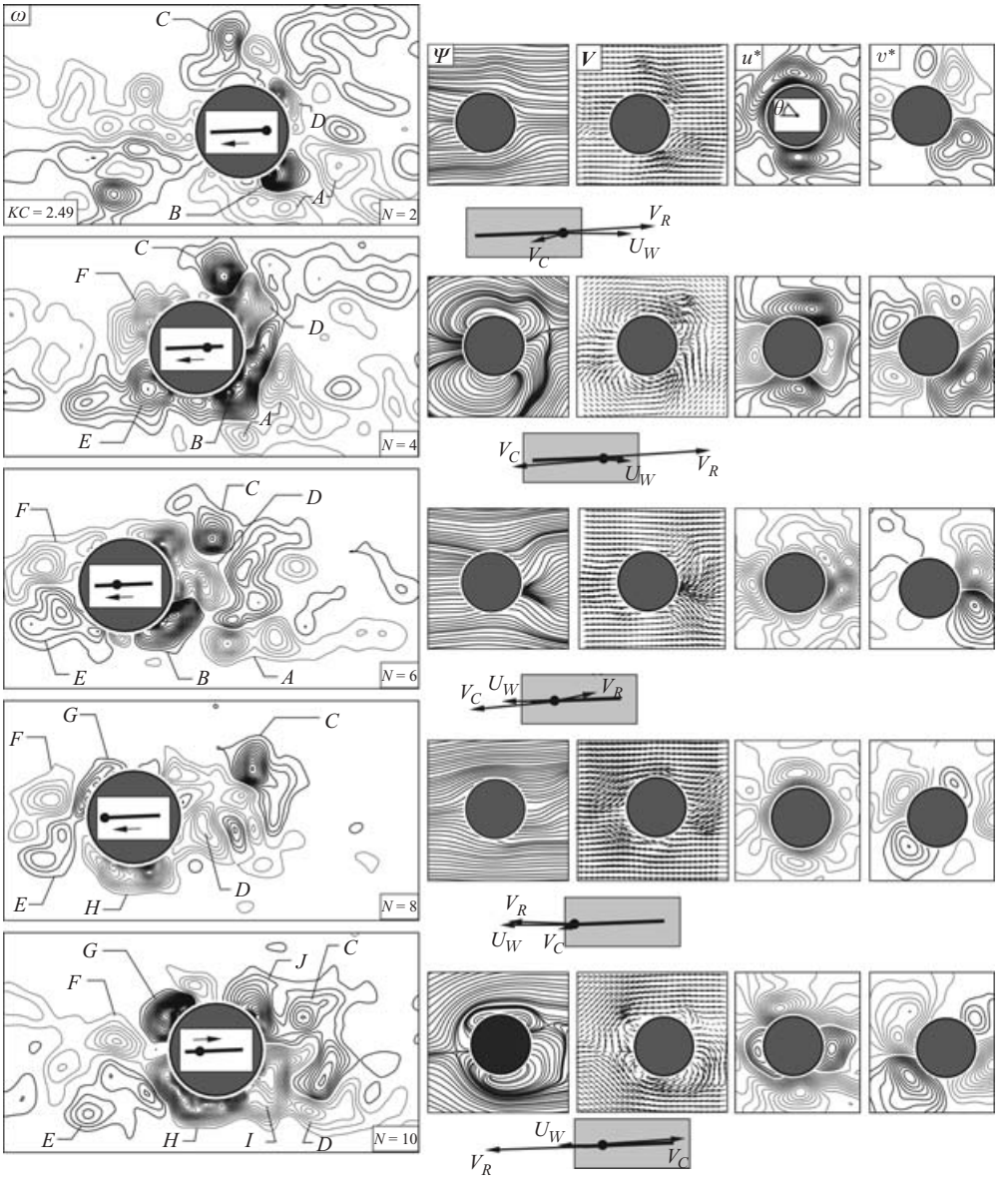

FIGURE 12. Patterns of instantaneous flow structure during the oscillation cycle of a cylinder at $KC = 2.49$. At $N = 2$, the magnitude of the instantaneous wave velocity is $U_w = 47.2\,\mathrm{mm\,s^{-1}}$. For instantaneous vorticity ω,$[\omega]_{min}$ and $\Delta[\omega]$ are both $1\,\mathrm{s^{-1}}$. For patterns of dimensionless instantaneous streamwise velocity component u^* and transverse component v^*, $[u^*]_{min} = [v^*]_{min} = \Delta[u^*] = \Delta[v^*] = 0.075$.

asymmetrical, in accord with the asymmetry of the vorticity layers B and C from the surface of the cylinder.

The patterns of u^* and v^* in figure 13 show a pronounced region of negative u^*, which marks the initial stage of large-scale antisymmetrical vortex formation in the wake of a cylinder, evident by comparison with a pattern of instantaneous vorticity ω at $N = 4$. This transformation to a high degree of asymmetry of the near-wake vortices, which is evident at $N = 6$ in the patterns of ω, in turn corresponds to a

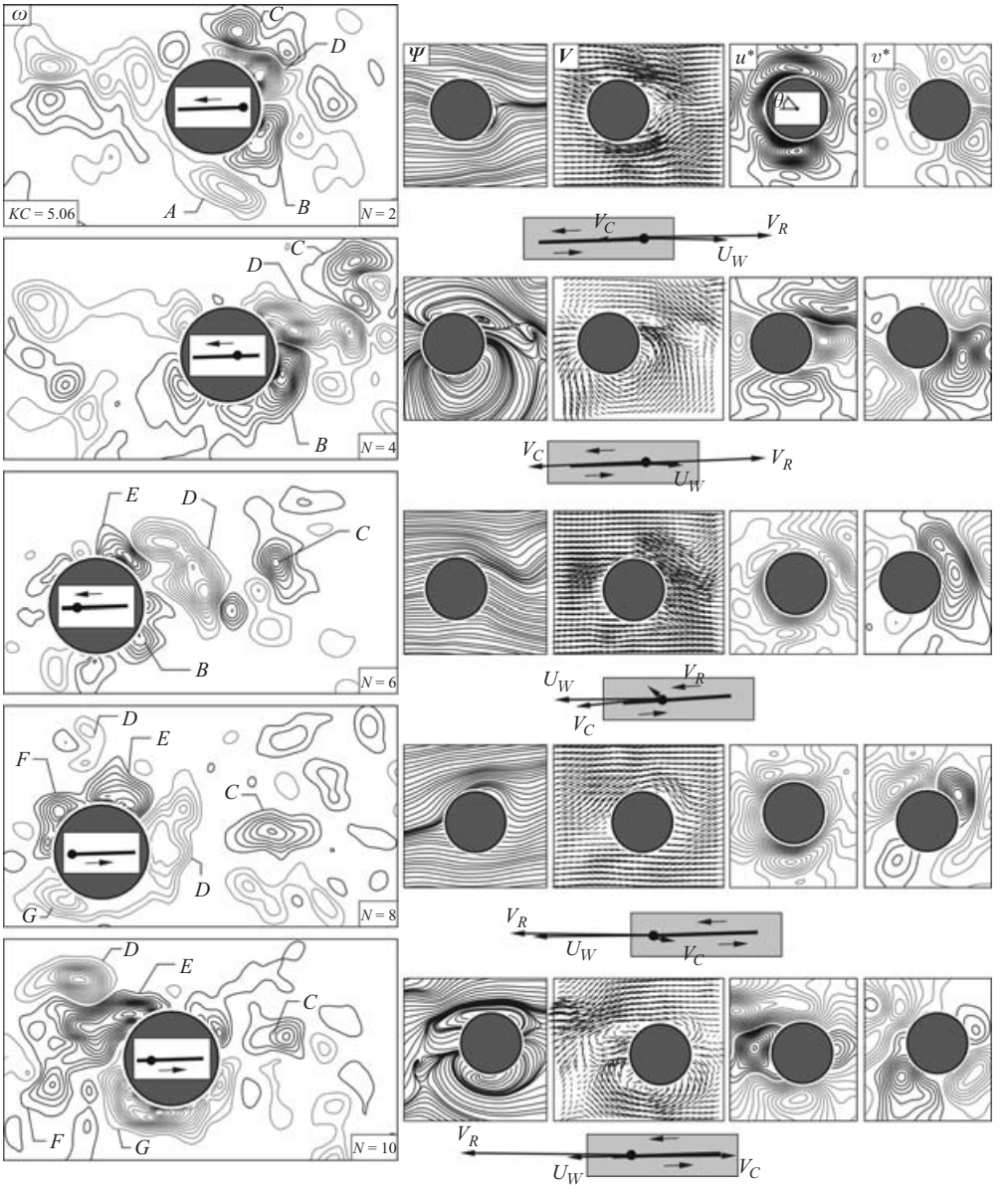

FIGURE 13. Patterns of instantaneous flow structure during the oscillation cycle of a cylinder at $KC = 5.06$. At $N = 2$, the magnitude of the instantaneous wave velocity is $U_w = 82.4\,\mathrm{mm\,s^{-1}}$. For instantaneous vorticity ω, $[\omega]_{min}$ and $\Delta[\omega]$ are both $3\,\mathrm{s^{-1}}$. For patterns of dimensionless instantaneous streamwise velocity component u^* and transverse component v^*, $[u^*]_{min} = [v^*]_{min} = \Delta[u^*] = \Delta[v^*] = 0.075$.

pattern of high-level vertical velocity v^* at $N = 6$ in the fifth column of images of figure 13.

6.3. *Elliptical and predominantly in-line trajectories: instantaneous and phase-averaged patterns*

Figure 14 provides a comparison of instantaneous and phase-averaged patterns of vorticity ω and $\langle\omega\rangle_p$, as well as streamlines ψ and $\langle\psi\rangle_p$, at each value of KC

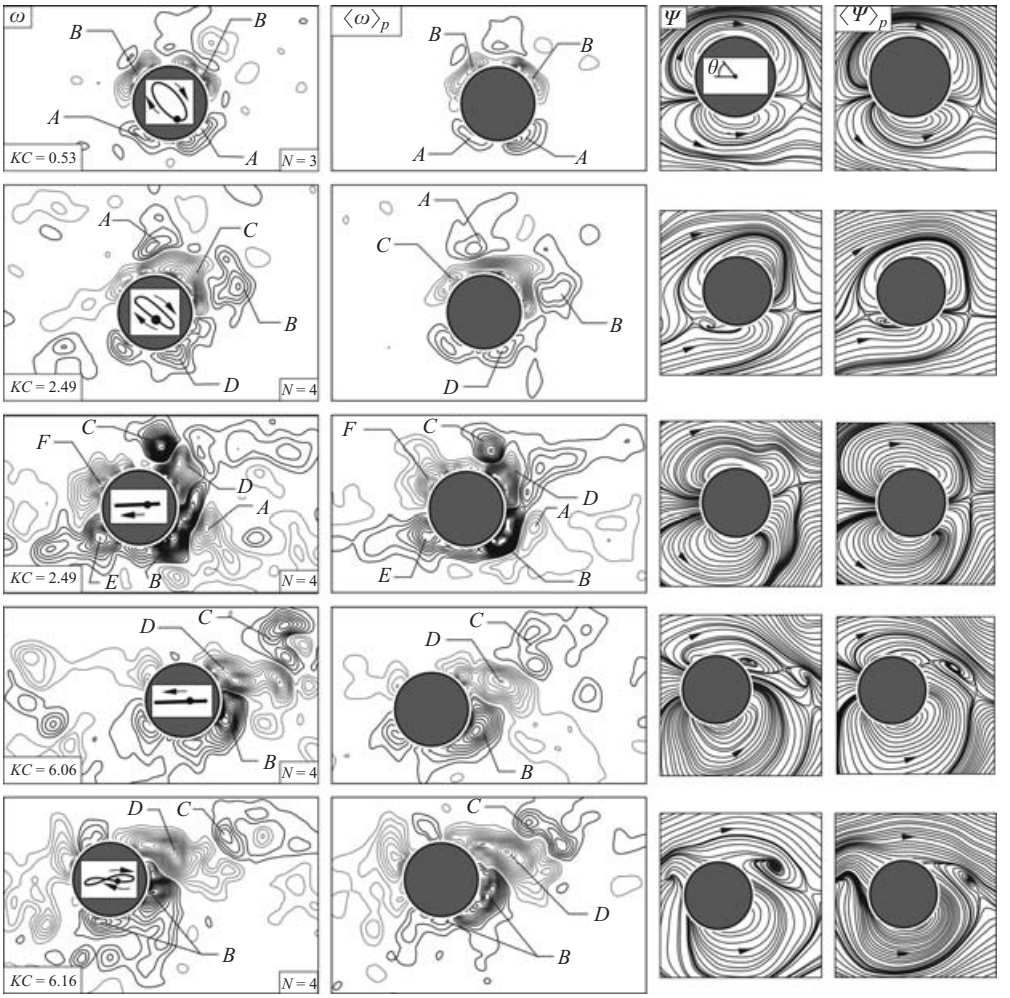

FIGURE 14. Comparison of instantaneous and phase-averaged patterns of vorticity and streamline topology for the oscillating cylinder at an instant corresponding to approximately the same streamwise position of the oscillation cycle. Minimum and incremental levels at each value of KC are the same as defined in figures 10 to 13 for $KC = 0.53$ to 5.06; levels at $KC = 6.16$ are the same as at 5.06.

considered herein and, furthermore, at approximately the same streamwise position of the cylinder trajectory. This streamwise position is designated by the solid dot in each of the trajectories shown in the patterns of vorticity ω. In essence, it corresponds to the initial stage of the leftward motion of the cylinder on its trajectory, irrespective of whether this trajectory is of an elliptical, linear, or figure-of-eight form. Comparison of each instantaneous pattern with its respective phase-averaged counterpart shows consistency of the major features of the patterns of vorticity, as well as the existence and approximate locations of critical points of streamline topology.

This set of images shown in figure 14 provides the opportunity to compare and define the major features of the flow pattern over the range of KC. At $KC = 0.53$, pronounced layers of vorticity occur about the upper and lower surfaces of the cylinder, and only low-level residual indications of vorticity are evident. They are

shed from a previous cycle(s) of the oscillations (see low-level concentrations of ω immediately above layer B).

At $KC = 2.49$ (elliptical trajectory), shown in the second row of figure 14, clusters of vorticity shed during the previous cycle of oscillation, designated as A and B, are evident; that is, they retain their identity after departure from the surface of the cylinder. These previously shed clusters A and B appear exterior to the distributed layer C. Generally speaking, however, no single large-scale cluster of vorticity departs significantly from the vicinity of the cylinder, i.e. it is not shed into the wake region during any part of the oscillation cycle.

In contrast, at $KC = 2.49$ (in-line trajectory), in the third row of figure 14, cluster C, which was shed during the preceding cycle, will, at later instants of time, move to a region to the right of the oscillating cylinder, as already depicted in figure 12. At $KC = 5.06$, shown in the fourth row of figure 14, a similar movement of cluster C, shed during a previous cycle to a substantial distance to the right of the cylinder, is already evident in the pattern of vorticity ω and, as shown in the sequence of figure 13, the cluster D will eventually be shed from the cylinder and move about its upper surface, towards the left-hand side, and into the wake region during the next half-cycle of the motion. Finally, the pattern of vorticity ω at $KC = 6.16$ in the fifth row of figure 14 shows a very similar form, including the previously shed concentration C and, as is evident by inspection of the complete sequence (not shown herein), cluster D is eventually shed to the left of the cylinder.

Remarkably, all of the patterns of ψ shown in figure 14 exhibit bubble-like regions, involving lines of separation and attachment. In a general sense, the locations of these bubble-like regions are consistent with pronounced layers or clusters of vorticity immediately adjacent to the cylinder and, furthermore, a given bubble contains vorticity of only a single sign.

7. Concluding remarks

This investigation focuses on characterization of the detailed flow patterns due to a vertical cylinder in a deep-water wave. Both the stationary and oscillating cylinder are considered. The elastic mounting system of the vertical cylinder allows very small values of the mass-damping ratio, as well as bidirectional oscillations, with no preference of stiffness or damping in the circumferential direction. Emphasis is on the range of KC extending from approximately 0.5 to 6; low and high values of KC within this range are referred to in the summaries that follow.

7.1. *Instantaneous patterns of flow structure: stationary cylinder*

For the case of the stationary cylinder, the flow patterns indicate remarkable symmetry with respect to the plane of symmetry of the cylinder, provided the value of KC is maintained sufficiently low. At high values of KC, however, within the range of $KC = 0.5$ to 6, the patterns of instantaneous vorticity during the wave cycle take on generic complex forms involving, for example, stacking of vorticity clusters across the near wake of the cylinder, as well as pronounced alternating shedding of large-scale vortical structures. All of these patterns from the stationary cylinder provide a basis for interpretation of the vorticity patterns and streamline topology arising from self-excited oscillations of the cylinder.

7.2. *Time-averaged patterns of flow structure: stationary cylinder*

The sequences of vorticity patterns during the wave oscillation cycle past the stationary cylinder, give rise to well-defined time-averaged patterns of the flow structure. Patterns

of time-averaged vorticity $\langle\omega\rangle$ show, at low KC, elongated layers on either side of the cylinder, and localized concentrations of vorticity immediately adjacent to its surface. At high values of KC within the range $KC = 0.5$ to 6, the pattern involves higher-level concentrations of vorticity near the surface of the cylinder; outboard of each of the respective concentrations, larger-scale lower-level patterns of vorticity of opposite sign exist in each respective quadrant. Corresponding patterns of root-mean-square vorticity ω_{rms} show a transformation from relatively distributed clusters at low KC, to well-defined concentrations at larger KC; these concentrations tend to occur close to the line of symmetry of the cylinder. Finally, patterns of time-averaged Reynolds stress correlation $\langle u'v'\rangle/U_m^2$ show, for all values of KC, remarkably similar patterns; peak values occur very close to the surface of the cylinder, obviously owing to the phase relationship between the streamwise u' and transverse v' fluctuations.

7.3. *Trajectories of oscillating cylinder*

Trajectories of the cylinder oscillation have been defined over the entire range of KC considered herein. At the lowest values of KC, the trajectory is a limit cycle in the form of an inclined ellipse; the transient development of the cylinder, starting from rest, has been characterized over a large number of wave cycles. At a critical value of KC, two admissible forms of the cylinder trajectory are evident: the aforementioned elliptical and a predominantly in-line mode. At high values of KC within the range $KC = 0.5$ to 6, the cylinder undergoes predominantly in-line motion. It therefore appears that a transitional state of the trajectory exists, from a predominantly elliptical trajectory at low KC to a predominantly in-line trajectory at higher values of KC. In this transitional state, elliptical and in-line trajectories are admissible.

7.4. *Patterns of instantaneous flow structure: oscillating cylinder*

Patterns of instantaneous vorticity ω, streamline topology ψ, as well as patterns of velocity vectors $\boldsymbol{V}$ and contours of constant streamwise u^* and transverse v^* velocity components, have been determined in relation to the instantaneous location of the cylinder on its trajectory. In addition, these patterns are interpreted in conjunction with the instantaneous wave velocity U_w, the cylinder velocity V_C, and the relative velocity V_R of the wave with respect to the cylinder. At low values of KC, for which the trajectory is elliptical, the vorticity layers are predominantly confined to the immediate vicinity of the cylinder, i.e. no clearly defined shedding occurs into the wake region. Well-defined clusters of positive and negative vorticity rotate about the cylinder, in accord with its elliptical trajectory, and therefore rotation of the relative velocity vector V_R. Furthermore, bubble-like patterns of streamlines are prevalent; each bubble contains nested streamlines that separate from, then reattach to the surface of the cylinder. The rotation of such bubbles about the surface of the cylinder is in accord with the aforementioned clusters of vorticity ω. The consequence of elevated, but still low KC, at which the elliptical trajectory is still maintained, is to allow clusters of vorticity shed during the previous cycle(s) to remain in the immediate vicinity of the cylinder.

In contrast to the elliptical trajectory of the cylinder, in-line trajectories, which occur at high values of KC within the range $KC = 0.5$ to 6, yield distinctly different, but generic classes of vorticity patterns; many of them are directly analogous to those occurring for the case of the stationary cylinder, and arise only for particular combinations of U_w, V_c and V_R. An important feature, for all of these values of KC, is the sweeping of a previously shed concentration of vorticity from one side of the cylinder to the opposite side, and into its near-wake region. At all values of KC, at

least one such sweep event occurs; at sufficiently high KC, two such events occur during the wave cycle.

7.5. *Spanwise variation of flow patterns: possibilities and consequences*

For the case of the deep-water wave investigated herein, the value of the KC number rapidly decreases along the span of the cylinder. The maximum value occurs immediately beneath the free surface, and at sufficiently large depth, a value of zero occurs. This spanwise variation has not been considered in the present investigation. Rather, a reference location close to the free surface, where the flow is highly energetic, has been taken to represent the predominant features of vortex formation and development. Interpretation of the quasi-two-dimensional patterns of vortex formation at this reference location is aided by closely related investigations of wave interaction with a stationary cylinder (Ozgoren & Rockwell 2004; Yang & Rockwell 2004), which address: (i) patterns of the spanwise variation of the three-dimensional flow structure; (ii) magnitude of the spanwise vorticity associated with quasi-two-dimensional vortex formation, relative to streamwise (wave direction) vorticity; and (iii) phase-referenced (locked) *vs.* modulated patterns of quasi-two-dimensional vortex formation as indicators of phase-locked three-dimensional patterns along the span of the cylinder.

Regarding interpretation of the flow patterns on a planar (horizontal) cut through the stationary cylinder, it is important to recognize, on the basis of the investigation of Yang & Rockwell (2004), that the peak levels of spanwise (vertically oriented) vorticity ω_z are at least an order of magnitude larger than the peak levels of streamwise (wave direction) vorticity ω_x. Owing to these relatively low levels of ω_x (and thereby circulation), sectional cuts of the flow structure, on planes orthogonal to the axis of the cylinder, provide a reasonable representation of the quasi-two-dimensional flow structure. (It should be noted that qualitative visualization, which has been employed extensively at low KC, indicates three-dimensionality of the flow, but does not indicate this remarkable difference of magnitude of orthogonal vorticity components.) Of course, with increasing distance from the free surface, the contributions to the cylinder loading will markedly decrease, because the peak vorticity ω_z, as well as the overall strength and phasing of the quasi-two-dimensional vortices, are substantially attenuated. For the present experiments, the total length of the cylinder L_{cyl}, normalized by its diameter D, is $L_{cyl}/D = 55.1$. The experiments of Yang & Rockwell (2004) and Ozgoren & Rockwell (2004) for the case of the stationary cylinder indicate that the spanwise extent of significant concentrations of ω_x, which is an indication of the extent over which pronounced shedding of spanwise vorticity ω_z occurs, is detectable over a distance of $10D$ to $12D$ from the free-surface at a value of $KC = 7$. Shedding therefore occurs over approximately one-fifth of the cylinder span. Moreover, contours of constant cross-wake velocity v(phase-averaged patterns) indicate that the shedding process, over this distance of $10D$ to 12 D, does not alternate sign, unlike cases of higher KC number.

Concerning the response of the oscillating (elastically mounted) cylinder, it is desirable to account fully for the spanwise variation of the flow structure, i.e. the instantaneous patterns of vortex formation at successively larger depths. It is expected, however, that the limit-cycle oscillations of the cylinder will tend to enhance the spanwise correlation of the flow structure. The instantaneous and phase-averaged patterns of quasi-two-dimensional vortex formation from the oscillating cylinder, shown in figure 14 for an inline trajectory, are in close agreement; when this is not the case, as shown by Ozgoren & Rockwell (2004) and Yang & Rockwell (2004),

significant variations (with space and time) of the spanwise flow structure occur during successive cycles of the wave motion. Generally speaking, the precise nature of the spanwise three-dimensionality, as a function of both the type of limit-cycle trajectory and the instantaneous location along the trajectory, requires further investigation.

A further point for investigation is the effect of the wavelength-to-depth ratio of the deep-water wave. As indicated, the present study is for the limiting case where pronounced shedding of vorticity (for the reference case of the stationary cylinder) occurs over a relatively small fraction (one-fifth) of the cylinder span. The wavelength-to-depth ratio may influence the cylinder trajectory. The basic types of trajectory of the cylinder motion, i.e. in-line, figure-of-eight, and orbital (elliptical) observed herein are, however, generic to a wide range of wave–cylinder parameters in related studies cited in § 1, where emphasis has not been on the associated flow structure. The present investigation establishes a one-to-one relationship between the phase-repetitive patterns of vortex formation on the reference plane immediately beneath the free surface and the trajectories of the cylinder motion.

The financial support of the Office of Naval Research, Grant N00014-94-1-0185, monitored by Dr Thomas Swean, is gratefully acknowledged.

REFERENCES

Adrian, R. J. 1991 Particle-imaging techniques for experimental fluid mechanics. *Annu. Rev. Fluid Mech.* **23**, 261–304.

Anagnostopoulos, P., Iliadis, G. & Ganoulis, J. 1995 Flow and response parameters of a circular cylinder vibrating in-line with the oscillating stream. In *Flow-Induced Vibration* (ed. P. Bearman), pp. 167–179. Balkema.

Angrilli, F. & Cossalter, V. 1982 Transverse oscillations of a vertical pile in waves. *Trans. ASME* I: *J. Fluids Engng* **104**, 46–53.

Bearman, P. W., Graham, J. M. R., Naylor, P. & Obasaju, E. D. 1981 The role of vortices in oscillatory flow about bluff bodies. *Proc. Intl Symp. on Hydrodynamics and Ocean Engineering* (The Norwegian Institute of Technology), pp. 621–644.

Bearman, P. W. & Hall, P. F. 1987 Dynamic response of circular cylinders in oscillatory flow and waves. In *Proc. BHRA Conf. on Flow-Induced Vibrations* pp. 183–190. *Bowness-on-Windemere, UK* (ed. R. King), BHRA, Cranfield.

Borthwick, A. G. L. & Herbert, D. M. 1988 Loading and response of a small diameter flexibly mounted cylinder in waves. *J. Fluids Struct.* **2**, 479–501.

Downes, K. & Rockwell, D. 2003 Oscillations of a vertical elastically-mounted cylinder in waves: imaging of vortex patterns. *J. Fluids Struct.* **17**, 1017–1033.

Dütsch, H., Durst, F., Becker, S. & Lienhart, H. 1998 Low-Reynolds-number flow around an oscillating circular cylinder at low Keulegan–Carpenter numbers. *J Fluid Mech.* **360**, 249–271.

Elston, J. R., Sheridan, J. & Blackburn, H. 2004 Two dimensional Floquet stability analysis of the flow produced by an oscillating circular cylinder in quiescent fluid. *Eur. J. Mech.* B/*Fluids* **23**, 99–106.

Guilmineu, E. & Queutey, P. 2002 A numerical simulation of vortex shedding from an oscillating circular cylinder. *J. Fluids Struct.* **16**, 773–794.

Hayashi, K. & Chaplin, J. R. 1998 Vortex-excited vibration of a vertical circular cylinder in waves. *Intl J. Offshore Polar Engng* **8**, 66–73.

Heinzer, A. & Dalton, C. 1969 Wake observations for oscillating cylinders. *Trans. ASME* D: *J. Basic Engng* 850–853.

Honji, H. 1981 Streaked flow around an oscillating circular cylinder. *J. Fluid Mech.* **107**, 509–520.

Ikeda, S. & Yamamoto, Y. 1981 Lift force on cylinders in oscillatory flows. *Rep. Dept of Found. Engng* and *Const. Engng (Saitama University)*, no. 10.

Isaacson, M. & Maull, D. J. 1981 Dynamic response of vertical piles in waves. *Intl Symp. on Hydrodynamics in Ocean Engineering (The Norwegian Institute of Technology),* pp. 887–904.

Iwagaki, Y., Asano, T. & Nagai, F. 1983 Hydrodynamic forces on a circular cylinder placed in wave-current co-existing fields. *Memo Faculty of Engineering (Kyoto University, Japan)* **45**, 11–23.

Kaye, D. 1989 Oscillation of a vertical cylinder in waves. PhD dissertation, University of Cambridge.

Kaye, D. & Maull, D. J. 1993 The response of a vertical cylinder in waves. *J. Fluids Struct.* **7**, 867–896.

Kozakiewicz, A., Sumer, B. M. & Fredsøe, J. 1997 Vortex regimes around a freely vibrating cylinder in oscillatory flow. *Intl J. Offshore Polar Engrs* **7**, 1053–5381.

Li, Y. S., Zhan, S. & Lau, S. L. 1997 In-line response of a horizontal cylinder in regular and random waves. *J. Fluids Struct.* **11**, 73–87.

Lin, X. W., Bearman, P. W. & Graham, J. M. R. 1996 A numerical study of oscillatory flow about a circular cylinder for low values of Beta parameter. *J. Fluids Struct.* **10**, 501–526.

Lipsett, A. W. & Williamson, I. D. 1991 Modelling the response of flexibly mounted cylinders in oscillatory flow. *Proc. First Intl Offshore and Polar Engineering Conf.* pp. 370–377.

Lipsett, A. W. & Williamson, I. D. 1994 Response of a cylinder in oscillatory flow. *J. Fluids Struct.* **8**, 681–709.

Obasaju, E. D., Bearman, P. W. & Graham, J. M. R. 1988 A study of forces, circulation and vortex patterns around a circular cylinder in oscillating flow. *J. Fluid Mech.* **196**, 467–494.

Ozgoren, M. & Rockwell, D. 2004 Interaction of a deep-water wave with a vertical cylinder at low *KC* number transition from phase-locked modes of vortex formation. *Phys. Fluids* **16**, 2700–2703.

Raffel, M., Willert, C. & Kompenhans, J. 1998 *Particle Image Velocimetry: A Practical Guide* Springer.

Sarpkaya, T. 1986 Force on a circular cylinder in viscous oscillatory flow at low Keulegan–Carpenter numbers. *J. Fluid Mech.* **165**, 61–71.

Sarpkaya, T. & Isaacson, M. De St. Q. 1981 *Mechanics of Wave Forces on Offshore Structures.* Van Nostrand Reinhold.

Sarpkaya, T. & Rajabi, F. 1979 Dynamic response of piles to vortex shedding in oscillating flows. *Eleventh Annual Offshore Technol. Conf. (OTC) 3647 Houston, TX*, pp. 2523–2528.

Sawaragi, T., Nakamura, T. & Miki, H. 1977 Dynamic behavior of a circular pile due to eddy shedding in waves. *Coastal Engng Japan* **20**, 109–120.

Sumer, B. M. & FredsøE, J. 1988 Transverse vibrations of an elastically mounted cylinder exposed to an oscillating flow. *J. Offshore Mech. Arctic Engng* **110**, 387–394.

Sumer, B. M. & Fredsøe, J. 1997 Hydrodynamics around cylindrical structures. *World Scientific.*

Sun, X. & Dalton, C. 1996 Application of the LES method to the oscillating flow past a circular cylinder. *J. Fluids Struct.* **10**, 851–872.

Tatsuno, M. & Bearman, P. W. 1990 A visual study of the flow around an oscillating circular cylinder at low Keulegan–Carpenter numbers and low Stokes numbers. *J. Fluid Mech.* **211**, 157–182.

Westerweel, J. 1993 Digital particle image velocimetry: theory and application. Doctoral Dissertation, Delft University.

Williamson, C. H. K. 1985*a* Sinusoidal flow relative to circular cylinders. *J. Fluid Mech.* **155**, 141–174.

Williamson, C. H. K. 1985*b* In-line response of a cylinder in oscillatory flow. *Appl. Ocean Res.* **7**, 97–106.

Yang, Y. & Rockwell, D. 2002 Wave interaction with a vertical cylinder: spanwise flow patterns and loading. *J. Fluid Mech.* **460**, 93–129.

Yang, Y. & Rockwell, D. 2004 Interaction of deep-water wave with a vertical cylinder: flow structure and loading. *J. Fluid Mech.* **520**, 267–295.

Zedan, M. F., Yeung, J. Y., Salane, H. J. & Fischer, F. J. 1981 Dynamic response of a cantilever pile to vortex shedding in regular waves. *Trans. ASME J. Energy Resources Technol.* **103**, 32–40.

Zhang, J. & Dalton, C. 1999 The onset of three dimensionality in an oscillating flow past a fixed circular cylinder. *Intl J. Numer. Meth. Fluids* **30**, 19–42.